Emerging Microbes & Infections
2025, VOL. 14, 2475836 (21 pages)
https://doi.org/10.1080/22221751.2025.2475836

Reverse genetics-derived cattle H5N1 virus from Clade 2.3.4.4b shows enhanced systemic infectivity and pathogenicity than an older Clade 1 H5N1 virus in BALB/c mice

Na Xiao[a]*, Xiang Yong Oong[a,b]*, Yanxia Chen[a,b], Can Li[a,b], Howard Chun-Ho Chung[a,b], Pui Wang[a,b], Zhanhong Ye[a,b], Alvin Hiu-Chung Lam[a,b], Jianpiao Cai[a,b], Wenchen Song[a], Andrew Chak-Yiu Lee[a,b], Hin Chu[a,b], Kin-Hang Kok[a,b], Jasper Fuk-Woo Chan[a,b,c,d], Shuofeng Yuan[a,b], Honglin Chen[a,b], Kwok-Yung Yuen[a,b,c,d] and Anna Jin-Xia Zhang[a,b]

[a]State Key Laboratory of Emerging Infectious Diseases, Carol Yu Centre for Infection, Department of Microbiology, School of Clinical Medicine, Li Ka Shing Faculty of Medicine, The University of Hong Kong, Pokfulam, Hong Kong Special Administrative Region, People's Republic of China; [b]Centre for Virology, Vaccinology and Therapeutics, Hong Kong Science and Technology Park, Hong Kong Special Administrative Region, Shatin, People's Republic of China; [c]Department of Microbiology, Queen Mary Hospital, Pokfulam, Hong Kong Special Administrative Region, People's Republic of China; [d]Department of Infectious Diseases and Microbiology, The University of Hong Kong-Shenzhen Hospital, Shenzhen, People's Republic of China

ABSTRACT

The newly emerged avian influenza A H5N1 Clade 2.3.4.4b can infect dairy cows and shed live virus in their milk. Sporadic cattle-to-human infections have been reported, highlighting the urgent need to understand its pathogenesis in mammals. Using both non-lactating and lactating BALB/c mice, we examined the viral tissue tropism, histopathological damages, and host immune responses upon intranasal inoculation with a reverse-genetic virus constructed based on A/dairy cattle/Texas/24-008749-003/2024 (Cattle-H5N1) and comparing with an older reference Clade 1 virus, A/Vietnam/1194/2004 virus (VNM1194-H5N1). Cattle-H5N1 was highly lethal in mice (mLD_{50} = 1.48PFU) with broad tissue tropism and produced higher titer in respiratory tissue and multiple extrapulmonary organs than VNM1194-H5N1. In the lungs, Cattle-H5N1 infection of airway epithelium, type II pneumocytes and $CD45^+$ immune cells were at a higher frequency than those of VNM1194-H5N1-infected mice, resulting in severe epithelial destruction and diffuse alveolar damage accompanied by elevated lung and serum pro-inflammatory cytokine/chemokines. Although both H5N1 viruses showed lactating mammary gland tropism, the gland tissue was more severely damaged after Cattle-H5N1 infection with abundant viral antigens expression in glandular cells, associated fat and lymphoid tissues. Furthermore, more suckling mice co-housed with Cattle-H5N1 infected lactating mice were virus-positive (7/30 pups) than VNM1194-H5N1. Brains were heavily infected by Cattle-H5N1, and neurological signs such as body-rolling/spinning, trembling and/or limb paralysis were seen only in Cattle-H5N1 infected mice. The spleen was more severely damaged by Cattle-H5N1 infection, which showed massive viral antigen expression accompanied by severe apoptosis and splenic atrophy, concluding that Cattle-H5N1 is more virulent in mice than VNM1194-H5N1.

ARTICLE HISTORY Received 12 September 2024; Revised 19 February 2025; Accepted 28 February 2025

KEYWORDS Clade 2.3.4.4b; H5N1; cattle; BALB/c mice; mammary gland; pathogenesis

Introduction

For over 20 years, the avian influenza A H5N1 virus has occasionally jumped host barriers to cause infection in mammals, including 909 sporadic cases of human infection from 1997 to April 2024 [1, 2]. Compared to other avian influenza subtypes (such as H7, H9, and H10), the H5N1 strain has been the most virulent for humans, with a case fatality rate of more than 50% [3]. Although the A/goose/Guangdong/1/96 (Gs/GD) strain, isolated in 1996, is the ancestor of the highly pathogenic avian influenza (HPAI) of the H5 subtype [4], the first documented cross-species transmission case of an H5N1 human infection in Hong Kong was in 1997, represented by A/Hong Kong/156/97 [5]. Following their initial emergence, the HPAI viruses continued to evolve through reassortment with low-pathogenicity avian influenza (LPAI) viruses and underwent further adaptive mutations to generate 10 distinct actively circulating clades that spread in 23 countries across Asia, Africa, the Middle East, and Europe [6, 7].

From 2020 to 2021, the genetic subgroup Clade 2.3.4.4b of H5N1, classified under Clade 2, emerged

CONTACT Anna Jin-Xia Zhang zhangajx@hku.hk; Honglin Chen hlchen@hku.hk State Key Laboratory of Emerging Infectious Diseases, Carol Yu Centre for Infection, Department of Microbiology, School of Clinical Medicine, Li Ka Shing Faculty of Medicine, The University of Hong Kong, Pokfulam, Hong Kong Special Administrative Region, People's Republic of China; Centre for Virology, Vaccinology and Therapeutics, Hong Kong Science and Technology Park, Hong Kong Special Administrative Region, Shatin, People's Republic of China
*These are co-first authors.

Supplemental data for this article can be accessed online at https://doi.org/10.1080/22221751.2025.2475836.

and rapidly spread across North and South America [8, 9]. In addition to infecting wild and domestic bird populations, viruses from this subgroup have also caused severe disease in various marine and terrestrial mammals [10–12]. However, the infection of H5N1 Clade 2.3.4.4b raised public health concerns when the virus was detected for the first time in the respiratory specimens, mammary gland tissues and unpasteurized milk samples of dairy cattle in the United States [13] and the first H5N1 cattle-to-human transmission was confirmed in 2024 [14]. The ongoing outbreak of H5N1 in cattle continues to affect a growing number of dairy farm workers who reported conjunctivitis and eye tearing [2], apart from the typical flu symptoms of fever, chills, coughing, and sore throat/runny nose. The reported lesions of mastitis in cattle [13] and subconjunctival haemorrhage of infected dairy farm workers [14] suggest that the H5N1 Clade 2.3.4.4b virus might have unusual tissue tropism besides replication in respiratory tissues, highlighting the need for further research in this area.

Recently, Eisfeld et al. (2024) examined the tissue tropism of A/dairy cattle/New Mexico/A240920343-93/2024 virus, an HPAI H5N1 Clade 2.3.4.4b genotype B3.13 virus isolated from infected cow milk, in female BALB/c mice and ferrets [15]. By comparing it with a typical avian H5N1 human isolate, A/Vietnam/1203/2004 (from Clade 1) [16], the authors found that both viruses can cause infections in respiratory and non-respiratory tissues by detecting viral load in the eye, mammary gland, teat, and brain. Avian H5N1 virus has been shown to cause extrapulmonary infection in mice, such as the brain [17].

To further elucidate the tissue tropism and histopathological characteristics caused by the newly emerging H5N1 cattle isolates from Clade 2.3.4.4b genotype B3.13, we infected female BALB/c mice, including lactating and nonlactating with a reverse genetically constructed virus, A/dairy cattle/Texas/24-008749-003/2024. We compared it with another distantly related H5N1 virus, A/Vietnam/1194/2004 (from Clade 1). We observed significant differences in replication kinetics and histopathology between the two viruses in various organs of the infected mice and the ability of the Cattle-H5N1 virus to disseminate to multiple extrapulmonary organs and induce dysregulated inflammation.

Materials and methods

Virus, cell lines and biosafety

A cattle-derived H5N1 virus from Clade 2.3.4.4b genotype B3.13 were constructed by reverse genetics based on publicly available genome sequences of A/dairy cattle/Texas/24-008749-003/2024 [13, 18]. Ethical approval was obtained for this study (No. FMBP3-098). The rescued virus (designated as Cattle-H5N1) was verified by whole genome Sanger sequencing in our laboratory, with the coding regions of each viral gene identical to the original isolate. The viral gene sequences (PB2, PB1, PA, NP, HA, NA, MP, NS) were submitted to NCBI GenBank with the accession numbers PQ898029–PQ898036. Concurrently, a Clade 1 H5N1 virus used in this study, A/Vietnam/1194/2004 (VNM1194-H5N1), was an old laboratory strain previously reported [19]. The viruses for mouse infection experiments were propagated and titrated on Madin-Darby Canine Kidney cells (MDCK) (ATCC® CCL-34™) cells for plaque-forming unit (PFU) and 50% tissue culture infectious dose ($TCID_{50}$) as previously described [20]. The virus stocks were stored at −80°C for later use. The generation of the H5N1 viruses by reverse genetics was assessed and approved by the Institutional Biological Safety Committee. Experiments involving infectious H5N1 virus were performed following the approved standard operating procedures of the Biosafety Level 3 facility at the University of Hong Kong (HKU).

Animals

Six to eight weeks old female BALB/c mice and lactating BALB/c mice at 4 days of lactation with three to six of her pups were obtained from the Centre for Comparative Medicine Research (CCMR), HKU. The animals were housed in specific-pathogen-free (SPF) facilities with 12-hour light–dark cycles and standard pellet feed and water *ad libitum*. All the animal-related experimental procedures were performed according to the standard operating procedures as previously described [19] and were approved by the Committee on the Use of Live Animals in Teaching and Research of HKU (CULATR # 24-188).

Virus infection of mice

To determine the 50% mouse infection dose of Cattle-H5N1 virus, groups of 5 mice were intranasally inoculated with 20 µl of the virus at 500, 100, 20, 4 and 0.8 PFU, and body weight and survival were observed for 14 days after virus inoculation. For this pathogenesis study, BALB/c mice were randomly divided into groups for intranasal inoculation with 500 PFU or 20 PFU of Cattle-H5N1 or VNM1194-H5N1 in 20 µl volume per animal under anaesthesia of ketamine (150 mg/kg given intraperitoneally) and xylazine (10 mg/kg given intraperitoneally) as previously reported [21]. Mock-infection controls were given the same volume of PBS. The body weight and signs of diseases were monitored at 1-, 4- or 7-days post-infection (dpi) when all the animals were sacrificed at a humane endpoint by euthanising them through

intraperitoneal injection of pentobarbital sodium (100 mg/kg). Lung tissues, nasal turbinate, trachea, mammary gland, brain, spleen, intestine, eyes, heart, and blood serum from the sacrificed mice were collected for virological, histological, and immunological analyzes. The collected organs were separated into two sets: one fixed in 10% neutral formalin for histopathological study and another frozen at −80°C for RNA extraction.

Histopathological, immunohistochemical, and immunofluorescence staining of tissue sections and automated imaging analysis

Tissues collected were immediately fixed in 10% neutral formalin and then processed as paraffin-embedded blocks. 4μm-thick sections were stained with haematoxylin and eosin (H&E) for histopathological examination. Influenza A H5N1 nucleoprotein (NP) and cellular marker proteins such as surfactant protein C (SPC), olfactory marker protein (OMP), ionized calcium binding adaptor molecular 1 (Iba-1) and leukocyte common antigen (CD45) were detected by immunohistochemistry (IHC) or immunofluorescence (IF) staining using antibodies listed in Table S1. Lung cell DNA fragmentation was labeled using a Click-iT® Plus TUNEL assay kit (Invitrogen, USA) according to the manufacturer's instructions previously described [22]. All tissue sections were examined under light or fluorescence microscopy in a blinded fashion. The images were captured using an OLYMPUS BX53 semi-motorized fluorescence or bright-field microscope with a DP80 camera and proprietary cellSens Standard software (Olympus LS, Japan). Pathology scores 1, 2, and 3 were given according to mild, moderate, and severe pathological change in terms of alveolar wall oedema, alveolar fluid exudation, perivascular oedema, peribronchiolar infiltration and bronchiolar epithelial cell death. NP quantification was analyzed by QuPath from 10 random views of each slide. Co-localization images of double IF staining were captured by an LSM900 confocal microscope (Carl Zeiss, Germany).

Determination of viral gene copies and infectious viral titre in homogenized specimens

The fresh tissue specimens were first homogenized with RNA extraction buffer. Then, total RNA was extracted from 350 μl of supernatant of tissue homogenate using MiniBEST Universal RNA Extraction Kit (Takara Bio, USA), and reverse transcription was performed using the PrimeScript™ RT reagent kit (Takara Bio, USA) using influenza-specific UNI12 primer (5'-AGCAAAAGCAGG-3'). The cDNA was amplified by quantitative PCR (qPCR) using QuantiNova® Probe PCR Kit (Qiagen, Germany) or SYBR® Premix Ex Taq II Kit (Takara Bio, CA, USA) with universal primer for the influenza A matrix (M) gene (Table S2) on LightCycler® 480 System (Roche Diagnostics, Germany). The pUC57 plasmids containing the cloned M gene and β-actin (ACTB) gene fragment were applied as standard. The detection limit of this assay was 100 copies of the viral M gene per ml of tissue homogenates. The expression of the ACTB housekeeping gene was determined in parallel for RNA normalization. A 50% tissue culture infection ($TCID_{50}$) assay using MDCK cells was performed to determine infectious virus titre in homogenized tissue samples. Briefly, the samples were serially diluted 10-fold and inoculated into MDCK cells in a 96-well plate followed by 1-hour incubation at 37°C. The cells were further incubated for 72 hours, and the cytopathic effect (CPE) was examined. $TCID_{50}$ titres (which measure or estimate the viral dilutions needed to infect 50% of wells with cultured cells) were calculated using the Reed & Munch endpoint method [23, 24].

Determination of the expression of cytokine, chemokine, and interferon-stimulated genes in lung tissue

Total RNA extracted from lung tissue homogenate was reverse transcribed into cDNA as described above, and the mRNA expression level of cytokines, chemokines, and interferon-stimulated genes (ISGs) was determined by RT-qPCR with gene-specific primers listed in Table S2. The expression of the ACTB housekeeping gene was determined in parallel for RNA normalization. The expression of cytokine/chemokine genes was analyzed by the $\Delta\Delta C_t$ method [25], using mock control lung tissue as the baseline expression level.

Detection of cytokine and chemokine protein levels in lung tissue and serum by beads-based multiplex flow cytometry

The cytokine and chemokine protein levels in mouse serum and lung homogenate were determined by LEGENDplex™ bead-based immunoassay (BioLegend, USA) according to the manufacturer's instructions. Briefly, samples were incubated with a mixture of capture beads for 13 cytokines and chemokines. After washing, the samples were stained with a biotinylated detection antibody cocktail and streptavidin-phycoerythrin (SA-PE). The intensity of signals was detected by flow cytometer BD LSRFortessa™ X-20 Cell Analyzer (BD Biosciences, USA), and the amount of each cytokine was determined according to the individual standard curves using LEGENDplex™ Data Analysis Software (BioLegend, USA).

Flow cytometry analysis

Single-cell suspensions from lung or spleen tissue were freshly prepared and fixed with a 4% paraformaldehyde solution. To determine cell composition and infection rate, cells were permeabilised and then incubated with Fc-receptor blocker antibody (BioLegend, USA) before staining with monoclonal antibodies against cell surface markers and influenza nucleoprotein (NP) (Table S1). Single cells from lung tissues were stained with influenza NP-FITC, CD45-PerCP/Cy5.5, B220-Brilliant Violet 421™, B220-PE, CD3-FITC, CD3-PE/Cy7, anti-Prosurfactant Protein C (proSP-C), and Donkey anti-rabbit-PE antibodies. Single cells from the spleen were stained with influenza NP-FITC, CD45-PerCP/Cy5.5, B220-Brilliant Violet 421™, and CD3-PE/Cy7 antibodies. Mouse lung type II pneumocytes were identified as SPC^+ cells, leukocytes as $CD45^+$ cells, B cells as $CD45^+$ $B220^+$ cells, and T cells as $CD45^+$ $CD3^+$ cells. Data were acquired using the BD LSRFortessa™ X-20 Cell Analyzer (BD Biosciences, USA) and analyzed using FlowJo™ Software (BD Biosciences, USA).

In vitro virus infection

To determine the replication kinetics of Cattle-H5N1 or VNM1194-H5N1, the adenocarcinoma human alveolar basal epithelial cell line A549 (ATCC® CCL-185™) and Calu-3 (ATCC® HTB-55™) were infected by the viruses at a multiplicity of infection (MOI) of 0.1. The cell culture supernatants and cell lysates were collected at 0-, 6-, 24-, and 48-hours post-infection (hpi). The $TCID_{50}$ assay and the viral M gene RT-qPCR were performed to determine the viral load in the cell culture supernatants and lysates. The viral loads at different hpi were plotted on a logistic growth curve model ($y = \frac{L}{1 + e^{-K(x-x_o)}}$, where y is the viral load value at time x, x_o is the sigmoid midpoint, K is the logistic growth rate, and L is the maximum viral load value). The model was then used to determine the virus's growth/replicate rate based on computing the K value.

Statistical analysis

All data were analyzed with Prism 8.0 (GraphPad Software Inc). Statistical comparisons among different groups were performed using two-tailed Student's t-test, One-way or Two-way ANOVA, and Tukey's multiple comparisons tests. Data were checked for normal distribution using the D'Agostino, Anderson–Darling, Shapiro–Wilk, or Kolmogorov–Smirnov test [26]. P-value (p) < 0.05 was considered statistically significant and highlighted in all figures.

Results

Cattle-H5N1 and VNM1194-H5N1 viruses differ genetically and have different replication kinetics in vitro and in vivo

The Cattle-H5N1 isolated in 2024 was reconstructed by reverse genetics. A highly pathogenic virus A/Vietnam/1194/2004 (VNM1194-H5N1) which was well studied previously [27, 28], was used as a reference for better understanding the replication and pathogenesis of Cattle-H5N1 *in vitro* and *in vivo*. As these two H5N1 viruses are genetically quite distant from each other, the average percent identity of the amino acid sequences between these two viruses is only 93.6%, with the NA (88.9%) and M2 (86.4%) identity, while the polymerase proteins (PA, PB1, and PB2) showing more than 97% identity (Figure 1A). Even with 45 amino acid substitutions between the HA of Cattle-H5N1 and VNM1194-H5N1 (Table S3), the signature motif of the polybasic amino acid cleavage site remained in the Cattle-H5N1 virus with only one amino acid deletion. Notably, there are 20 amino acid insertions ("CNQSIIYENNTWVNQTYIN", position 49–68) in the NA, and 5 amino acid insertions ("TIASV"; position 80–84) on the NS1 protein of Cattle-H5N1 (Figure 1A), which was not observed in VNM1194-H5N1.

We studied the *in vitro* replication kinetics in human lung epithelial cell lines A549 and Calu-3. By measuring the viral load (M gene copy numbers and $TCID_{50}$) in the cell culture supernatant (Figure 1B and C), we found that Cattle-H5N1 replicated faster by having a significantly higher growth rate (mean K value = 0.1183 in A549, mean K value = 0.1245 in Calu-3) in both cell lines than VNM1194-H5N1 (mean K value = 0.0810 in A549, mean K value = 0.05125 in Calu-3), with statistical significance ($p < 0.05$) in a logistic growth function (Figure 1B and S2). The $TCID_{50}$ viral load results concurred with those obtained by measuring the M gene copy number (Figure 1C). This was further confirmed by measuring their M gene copy number in infected A549 and Calu-3 cell lysates (mean K = 0.2283 in A549 and 0.2073 in Calu-3 after Cattle-H5N1 infection vs mean K = 0.1242 in A549 and 0.1529 in Calu-3 after VNM1194-H5N1 infection, $p < 0.05$). These results suggested that the Cattle-H5N1 virus has acquired higher replication efficiency in human lung cell lines.

To study the pathogenicity, we infected groups of mice with different doses of Cattle-H5N1, 500, 100, 20, 4 and 0.8 PFU. Figure 1D shows the body weight changes and survival of the infected mice. The 50% mouse lethal dose (mLD_{50}) of Cattle-H5N1 was determined as 1.48 PFU. The mLD_{50} of VNM1194-H5N1 was previously determined as 20 PFU [29]. To further elucidate Cattle-H5N1 and VNM1194-H5N1

A

Protein	Percent amino acid identity (%)	Number of amino acid substitutions	Number of amino acid (aa) insertions/deletions
HA	91.8	45	1 - aa deletion in Cattle-H5N1
NA	88.9	32	20 - aa insertion in Cattle-H5N1
NS1	90.8	16	5 - aa insertion in Cattle-H5N1
NS2	92.8	9	
M1	93.2	17	
M2	86.4	13	
NP	98.5	7	
PA	97.9	15	
PB1	98.1	14	
PB2	97.7	17	

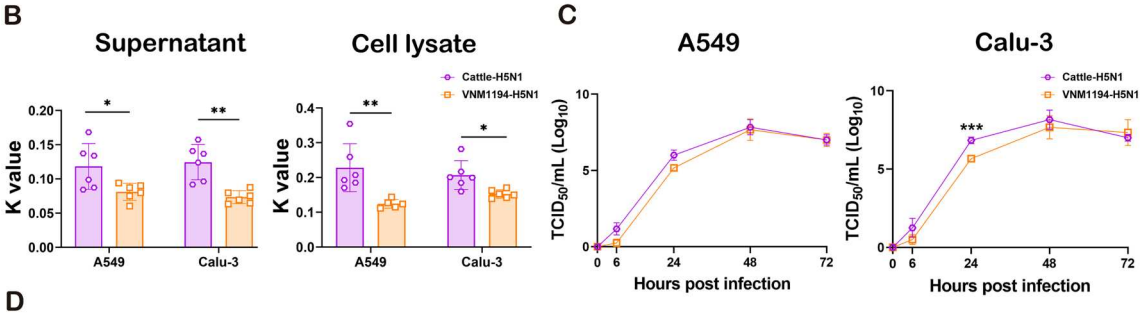

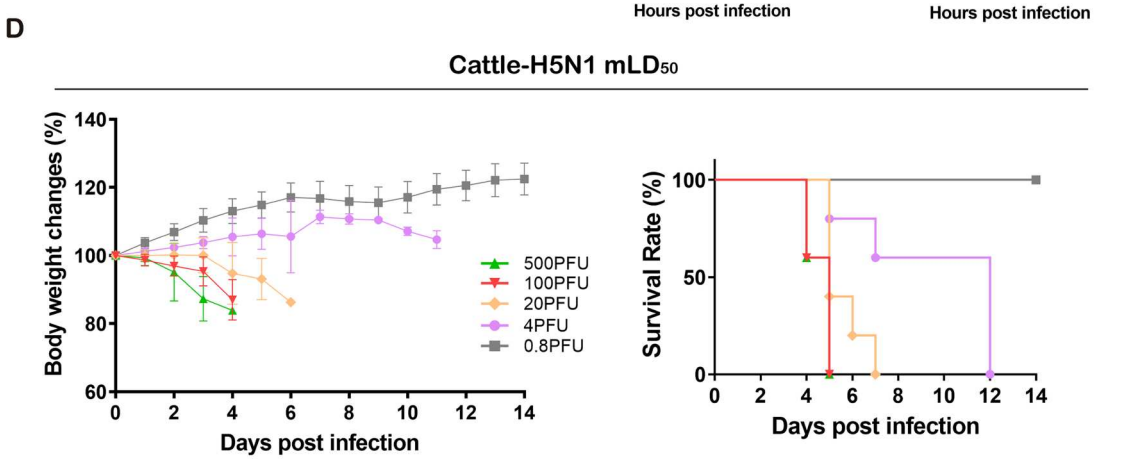

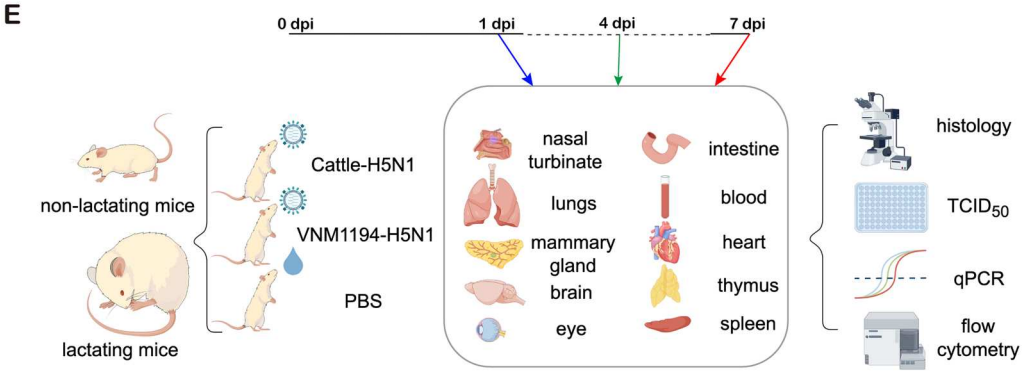

Figure 1. Virological profile of Cattle-H5N1 and VNM1194-H5N1. A. Percent identity and amino acid substitutions between Cattle-H5N1 and VNM1194-H5N1. B. Replication rate (K value) of Cattle-H5N1 and VNM1194-H5N1 in the supernatants and cell lysates after *in vitro* infection of A549 and Calu-3 cells with an MOI of 0.1. Data were shown as mean ± SD from 6 replicates (n = 6), where ** $p < 0.01$, *** $p < 0.001$ were determined by Two-tailed Student's *t*-test. C. Viral titer in the supernatants after *in vitro* infection of A549 and Calu-3 cells with an MOI of 0.1. Data were shown as mean ± SD from 6 replicates (n = 6), where *** $p < 0.001$ were determined by Two-tailed Student's *t*-test. D. The body weight changes and survival rate of Cattle-H5N1 LD50 test. The experimental layout to determine the pathogenicity of Cattle-H5N1 and VNM1194-H5N1 in BALB/c mice by Figdraw (https://www.figdraw.com/static/index.html#/). F. Body weight changes of BALB/c mice were monitored daily for 4 days after 500 PFU virus infection. Data shown were mean ± SD of five replicates (n = 5). G. Body weight changes of BALB/c mice were monitored daily for 14 days after 20 PFU virus infection. Data shown were mean ± SD of five replicates (n = 5), where * $p < 0.05$, **** $p < 0.0001$ were determined by Two-tailed Student's *t*-test. H. Survival rate after 20 PFU infection of Cattle-H5N1 and VNM1194-H5N1.

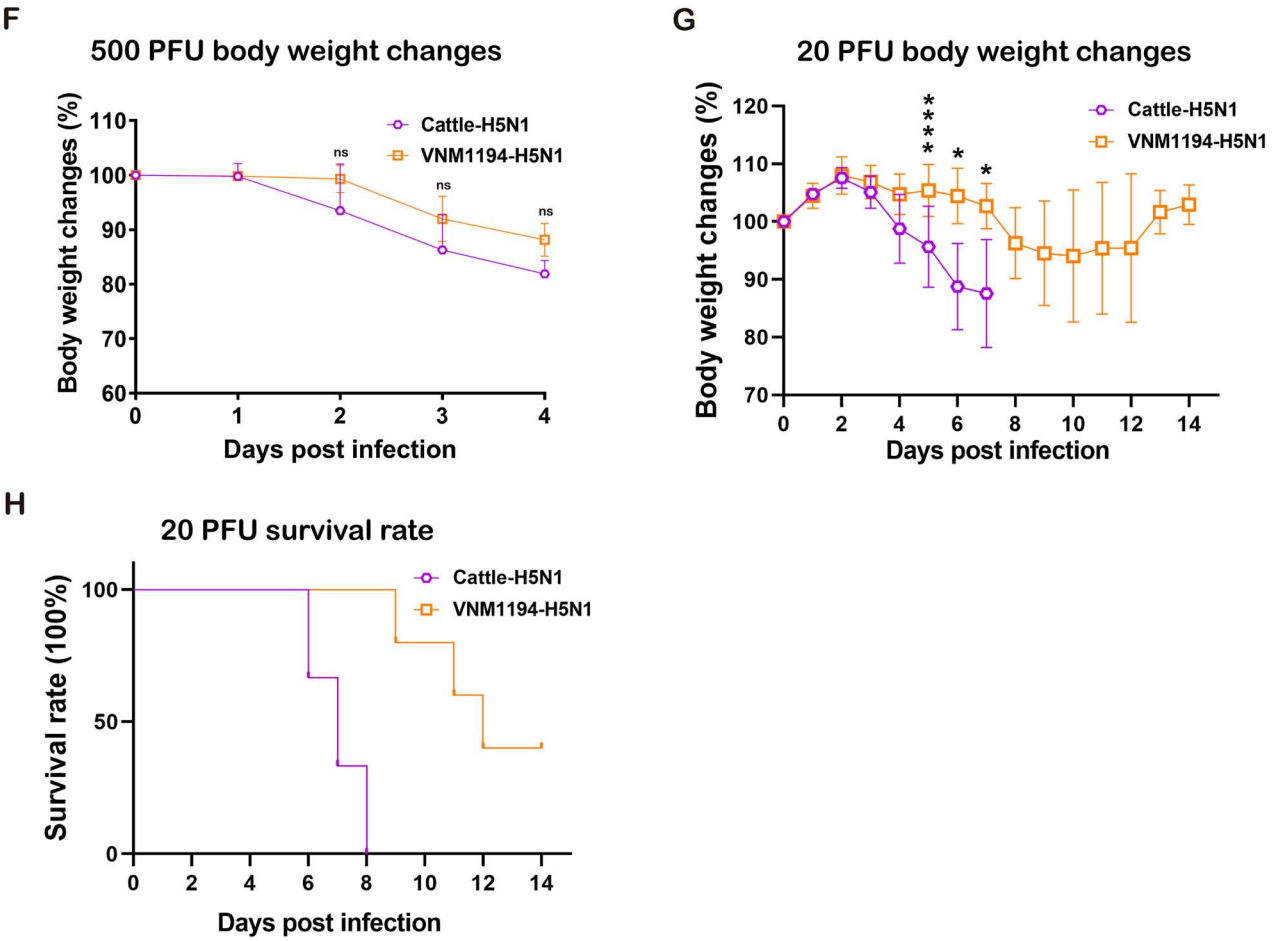

Figure 1. *Continued*

infection-induced histopathological changes in mice, the mice were inoculated with the highest lethal dose of 500 PFU. The animals were sacrificed at 1 or 4 dpi for virological, histological and immunological analysis (Figure 1E). During this monitoring process, we observed a more significant reduction in body weight of Cattle-H5N1-infected mice (18%) at 4 dpi than VNM1194-H5N1-infected mice (12%) (Figure 1F). At the same time, both infection groups exhibited comparable symptoms such as ruffled fur, hunched posture, and labored breathing without any signs of neurological damage during the 4-day observation period.

Since all Cattle-H5N1 infected mice died at 5 dpi after inoculation with 500 PFU (Figure 1D), we lowered the virus dose to 20 PFU to have a complete picture with a more prolonged course of infection. Three mice from each infection group (Cattle-H5N1 vs VNM1194-H5N1) were sacrificed at 4 or 7 dpi for further analyzes. As shown in Figure 1G on the body weight changes and Figure 1H on the survival rate, 20 PFU of Cattle-H5N1 caused aggressive weight loss from 5 to 7 dpi, which was significantly more compared to VNM1194-H5N1 ($p < 0.05$). All Cattle-H5N1 infected mice (5/5) died at 8 dpi, while 2/5 mice in the VNM1194-H5N1 infection group gradually recovered from infection at 14 dpi (Figure 1H). These results suggested that the Cattle-H5N1 virus are more virulent than VNM1194-H5N1 in BALB/c mouse model by having a lower mLD_{50}.

Cattle-H5N1 virus causes more severe damage to the nasal turbinate and lung tissues than VNM1194-H5N1

Virus replication in respiratory tissue was determined by qPCR determination of viral loads in the lung and nasal turbinate tissues. After 500 PFU inoculation, Cattle-H5N1 replicated to significantly higher titre in both nasal turbinate and lung tissues at 1 and 4 dpi compared to VNM1194-H5N1 (Figure 2A). Specifically, the $TCID_{50}$ titre of Cattle-H5N1 was 3 logs higher in nasal turbinate and 2 logs higher in the lungs of infected BALB/c mice at 4 dpi than VNM1194-H5N1 ($p < 0.01$). In 20 PFU of Cattle-H5N1 inoculated mouse lung and NT samples, the virus replicated to a titer as high as that of 500PFU infection at 4 dpi, and the viral load ($TCID_{50}$ and M gene copy number) did not further increase at 7 dpi (Figure 2B). In contrast, at 4 dpi, after 20 PFU of VNM1194-H5N1 inoculation, lung viral load was about 3 logs lower than 500 PFU infected lung at

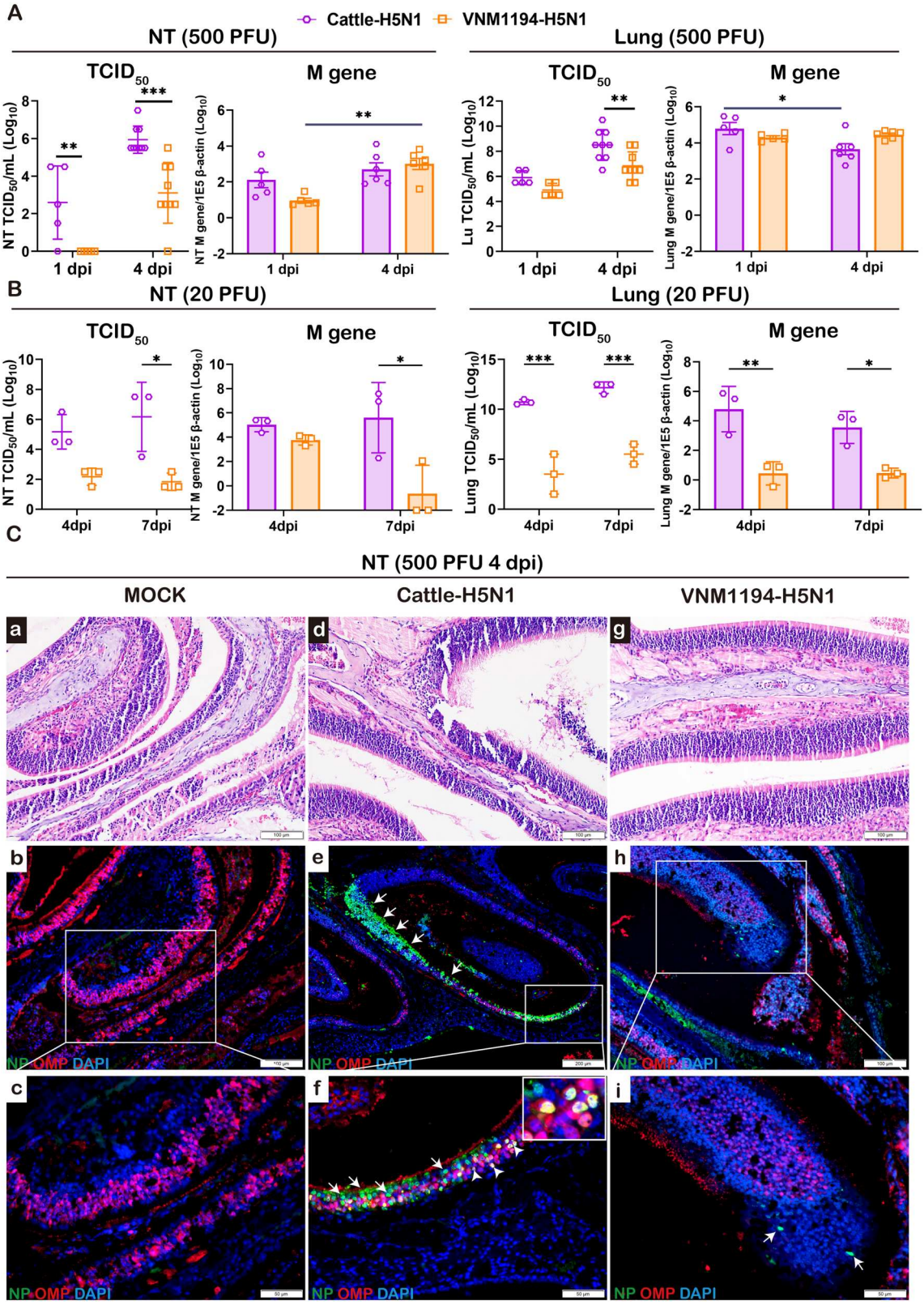

Figure 2. Viral titres in the nasal turbinate (NT) and lung tissues, and histopathological changes in the nasal turbinate (NT) of BALB/c mice after infection. A. Viral loads in nasal turbinate (NT) and lung tissues at 1 and 4dpi were determined by $TCID_{50}$ assay and viral M gene copy numbers in tissue homogenates. Data were shown as mean ± SD (n = 5 for 1 dpi data, n = 6 for 4 dpi PCR data, and n = 9 for 4 dpi $TCID_{50}$ data), where * $p < 0.05$, ** $p < 0.01$, *** $p < 0.001$ were determined by Two-way ANOVA with Tukey's multiple comparisons test. B. Viral loads in nasal turbinate (NT) and lung tissues at 4 and 7 dpi were determined by $TCID_{50}$ assay and viral M gene copy numbers in tissue homogenates. Data were shown as mean ± SD (n = 3), where * $p < 0.05$, ** $p < 0.01$, *** $p < 0.001$ were determined by Two-way ANOVA with Tukey's multiple comparisons test. C. Representative histological images (H&E-stained and IF-stained with anti-NP and anti-OMP) of mock and infected NT tissue sections at 4 dpi. White arrows indicate NP-positive cells. White arrowheads indicate double positive cells. Scale bar = 50μm or 100μm.

4 dpi. These data indicated that Cattle-H5N1 replicated more effectively in mouse lungs than VNM1194-H5N1, which needs a higher initial inoculation dose to reach a high titer in the lung.

The distribution of viral antigens in lung and NT tissue was examined by IHC and IF staining with anti-influenza NP antibodies. Cattle-H5N1 NP was found in both respiratory and olfactory epithelium (RE and OE, respectively) in the nasal turbinate, segmentally distributed along the pseudostratified epithelium involving multiple sites of the olfactory folding structures (Figure 2C, Figure S3). The NP-positive cells were more abundant at 4 dpi than 1 dpi after 500 PFU inoculation, and there was also a further increase from 4 to 7 dpi in the 20 PFU inoculation group. Furthermore, double immunofluorescence staining of olfactory marker protein (OMP) and NP antigens indicated that Cattle-H5N1 infected olfactory sensory neurons. In contrast, VNM1194-H5N1 infected nasal turbinate with only sporadic viral antigen-positive cells or small positive foci in RE or OE.

In the lungs, tissue damage was already visible microscopically at 1 dpi after 500 PFU Cattle-H5N1 or VNM1194-H5N1 inoculation, manifesting as perivascular inflammation and ballooning degeneration of bronchial epithelium, with more severe damage of alveoli observed in Cattle-H5N1 infection (Figure S4A). Cattle-H5N1 NP positive cells clustered as small foci in both bronchioles and distal alveoli affecting three lung lobes examined at 1 dpi, while limited VNM1194-H5N1 NP signals were observed in the bronchioles, not in alveoli (Figure S4A). At 4 dpi, Cattle-H5N1 infected lung manifested as diffuse alveolar damage, including alveolar wall oedema and alveolar sac fluid exudation (Figure 3A). Interstitially, prominent perivascular oedema, while not peribronchiolar infiltration, was observed despite severe bronchiolar epithelial cell death and depletion. Similarly, 20 PFU inoculation-induced mouse lung tissue damages were much milder than those caused by 500 PFU at 4 dpi, with the lung tissue mainly showing diffuse alveolar vesicular congestion, but an alveolar sac with diffuse protein-containing fluid was shown in the distal lung (Figure S4B). At 7 dpi, although the lung viral load did not further increase, the lung damage worsened as bronchiolar epithelium sloughing, diffuse alveolitis with alveolar infiltration, haemorrhage, and oedema (Figure S4B). In contrast, the VNM1194-H5N1 infection induced localized interstitial bronchopneumonia adjacent to severely damaged bronchioles, evidenced by epithelial cell sloughing and a large amount of luminal cell debris. Immune cell infiltration in the affected lung led to focal alveolar consolidation (Figure 3A), while no lung tissue consolidation was observed in Cattle-H5N1 infected lungs. 20 PFU of VNM1194-H5N1 inoculation caused even milder changes in the lung. The main feature was alveolar vessel congestion and infiltration without fluid accumulation in the alveolar sac. At 7 dpi, the lung damage also worsened as severe bronchiolar epithelium sloughing and massive immune cell infiltration sounding the damaged bronchioles, which formed localized lung tissue consolidation (Figure S4B).

Influenza NP antigen-positive cells in Cattle-H5N1 infected lungs increased massively at 4 dpi, compared to 1 dpi, which diffusely distributed in alveoli across every lung lobe examined (3 lobes per animal) (Figure 3B). In comparison, VNM1194-H5N1 NP antigen was patchily distributed in the alveoli adjacent to the affected bronchioles. Furthermore, through double IF staining of prosurfactant protein C (proSP-C) and NP antigen and flow cytometry analysis, we confirmed that there was a significantly higher percentage of NP^+ $proSP\text{-}C^+$ AT2 (mouse alveolar type II pneumocytes cells) in Cattle-H5N1 infected lungs (~50%) compared to VNM1194-H5N1 (~20%) (Figure 3C and D). Flow cytometry analysis also indicated that $CD45^+$ immune cells in Cattle-H5N1 infected lung frequently showed NP positive, 14.4% vs 2.4% in VNM1194-H5N1 infection (Figure 3D). This data indicates that Cattle-H5N1 infects lung epithelial cells and immune cells more efficiently. By IF staining lung tissues with anti-Iba-1 antibody, we also detected a lower amount of $Iba\text{-}1^+$ macrophages in Cattle-H5N1-infected lungs compared to VNM1194-H5N1 (Figure S6A). With significantly increased TUNEL positivity in Cattle-H5N1-infected lung tissue (Figure S6B), virus-induced massive cell death may be attributed to less adequate immune cell recruitment in the Cattle-H5N1-infected lung.

To further elucidate host innate immune responses to H5N1 infection in the lung, we determined the mRNA expression levels for interferons and key pro-inflammatory cytokine/chemokines. Both H5N1 viruses' infection upregulated TNF-α, IL-1β, IL-6, CXCL10, and CXCL2 at 1 dpi, among which Cattle-H5N1-infected lungs had slightly higher expression compared to VNM1194-H5N1 (Figure 3E). At 4 dpi, the expression of these cytokines further increased, with VNM1194-H5N1-infected lungs having 10/12 cytokines, which surpassed that of Cattle-H5N1-infected lungs. The expression of interferons also showed a similar pattern with IFN-α and IFN-β upregulated to a higher level than mock controls at 1 dpi. Their further increase at 4 dpi was also accompanied by elevated levels of IFN-γ, IFN-λ, and IL-28. The differences in mRNA levels of all 12 tested cytokines/chemokines in the lungs at 1 and 4 dpi were insignificant with both viruses (Figure 3E), except for the gene expressing monocyte chemoattractant protein 2 (also known as chemokine ligand 8, CCL8) at 4 dpi in which VNM1194-H5N1 showed significantly higher expression ($p < 0.01$).

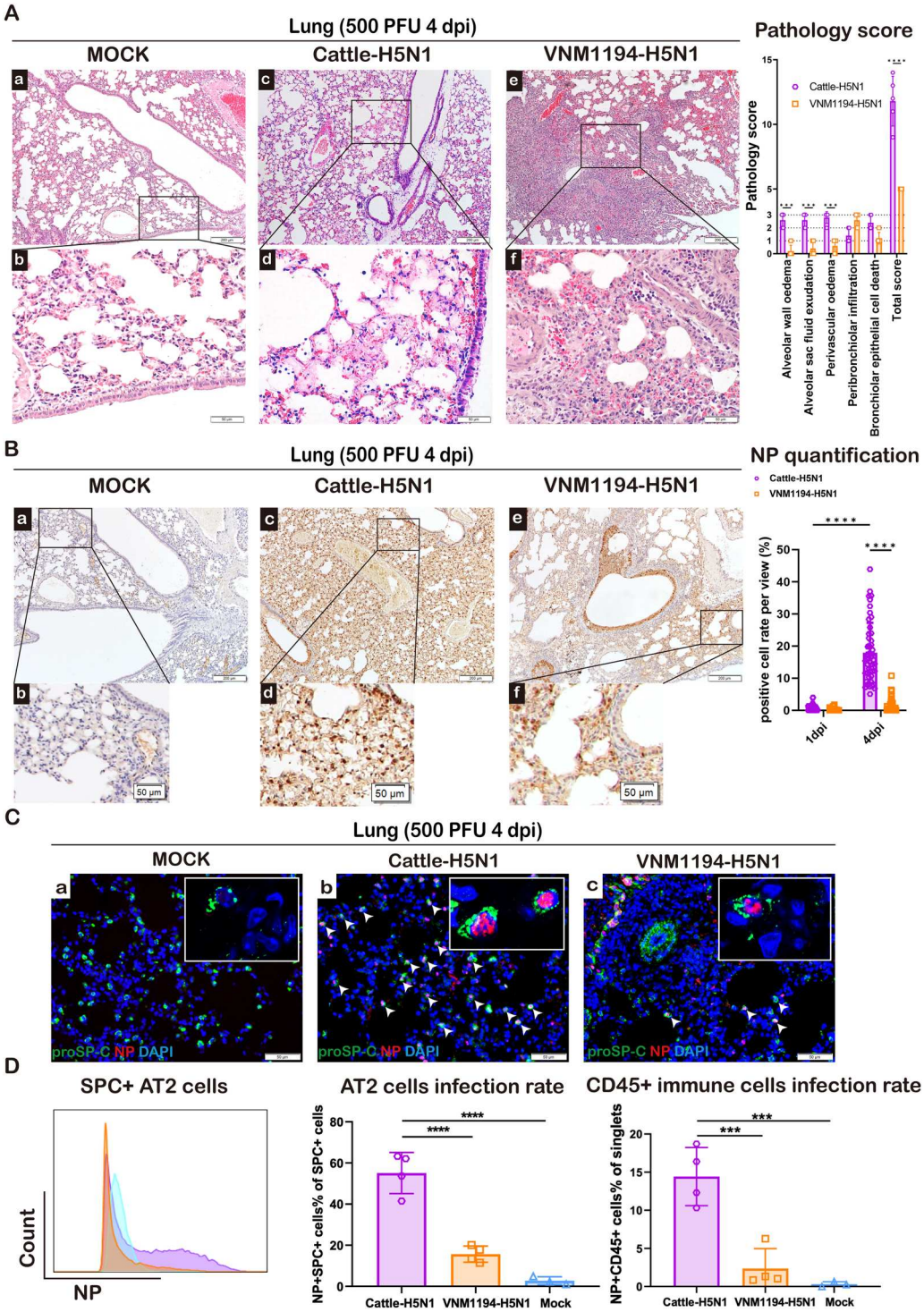

Figure 3. Histopathological changes and immunological profiles in the lung tissues of BALB/c mice after infection. A. Representative histological images (H&E-stained) of mock and infected lung tissues at 4 dpi and pathology score. Data were shown as mean ± SD (n = 5), where *** $p < 0.001$, **** $p < 0.0001$ were determined by Two-way ANOVA with Tukey's multiple comparisons test. B. Representative immunohistochemistry (IHC) images of mock and infected lung tissues at 4 dpi, and NP quantification of infected lungs at 1 and 4 dpi. Data were shown as mean ± SD (n = 50), where **** $p < 0.0001$ were determined by Two-way ANOVA with Tukey's multiple comparisons test. C. Representative histological images (IF-stained with anti-NP and anti-proSP-C) of mock and infected lung tissues at 4 dpi. White arrowheads indicate NP- and proSP-C double positive cells. D. Percentage of NP^+ SPC^+ mouse alveolar type II (AT2) pneumocytes and NP^+ $CD45^+$ immune cells by flow cytometry analysis after infection at 4 dpi. Data were shown as mean ± SD from three or four replicates (n = 3 for mock and n = 4 for infection group), where *** $p < 0.001$, **** $p < 0.0001$ were determined by One-way ANOVA with Tukey's multiple comparisons test. Scale bar = 50μm or 200μm. E. Relative mRNA expressions of selected cytokines and chemokines at 1 and 4dpi in mock and infected lung homogenates. RNA expression was normalized against the housekeeping gene ACTB. The data were shown as the mean ± SD from five replicates (n = 5), where * $p < 0.05$, ** $p < 0.01$, *** $p < 0.001$, **** $p < 0.0001$ were determined by One-way ANOVA with Tukey's multiple comparisons test. F. Selected cytokine and chemokine protein levels at 1 and 4 dpi presented in mock and infected lung homogenates. The data were shown as the mean ± SD from three or five replicates (n = 3 for mock and n = 5 for infection group), where * $p < 0.05$, ** $p < 0.01$, *** $p < 0.001$, **** $p < 0.0001$ were determined by One-way ANOVA with Tukey's multiple comparisons test.

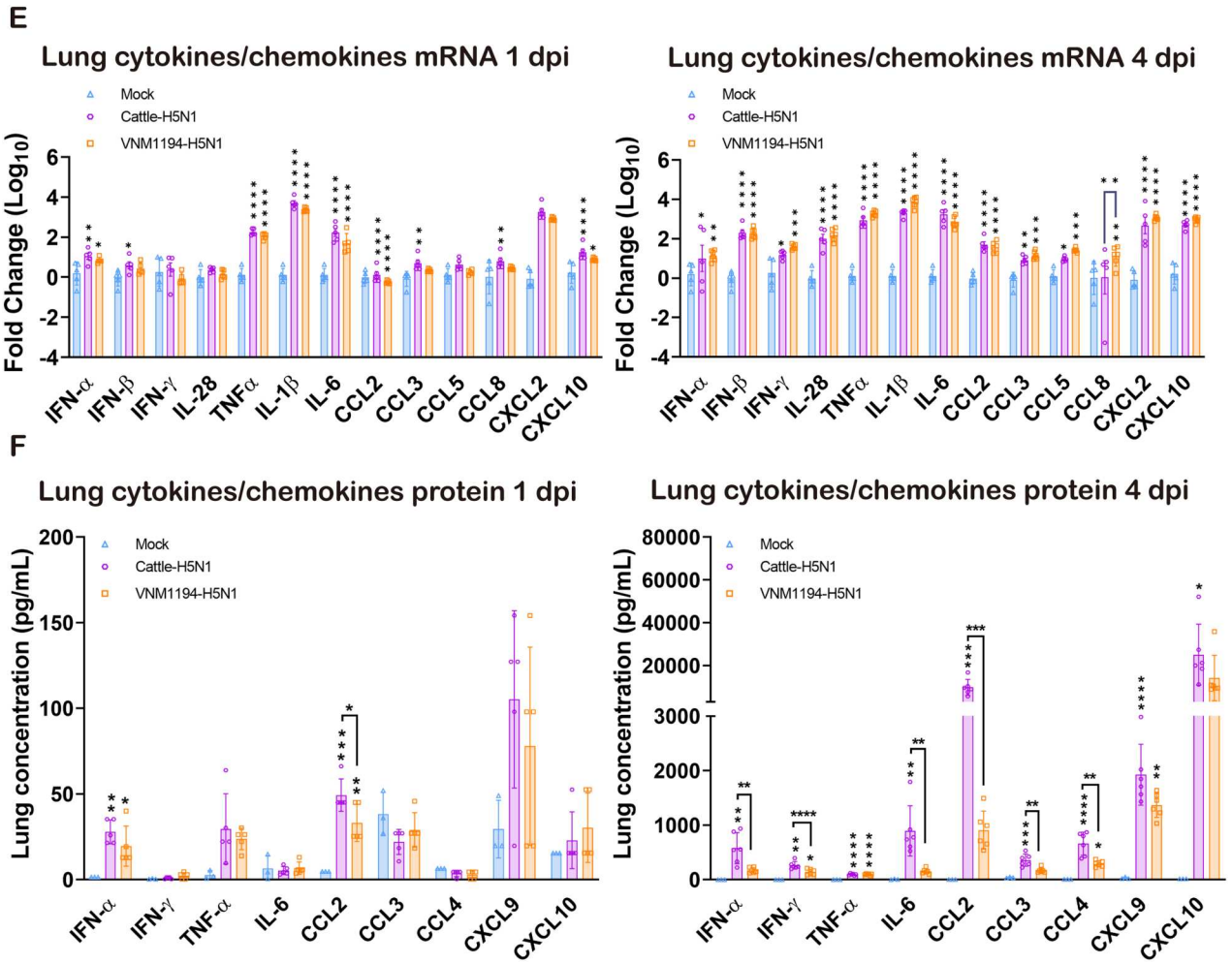

Figure 3. *Continued*

Similarly, for the mRNA expression of genes involved in innate immune signaling pathways or interferon-stimulated genes (ISGs), we only detected increased levels of STATs, OAS3, and MX1 in Cattle-H5N1-infected lungs at 1 dpi with significance ($p < 0.05$) compared to mock-infected lungs (Figure S5A). However, the expression of 8/12 ISGs in VNM1194-H5N1-infected lungs surpassed those from Cattle-H5N1 at 4 dpi, with OAS3 and MX1 showing significant differences ($p < 0.05$) (Figure S5B). At the protein level, the Cattle-H5N1 infection induced markedly higher concentration of key cytokines and chemokines in the lungs, including IFN-α, IFN-γ, IL-6, CCL2, CCL3, and CCL4, relative to VNM1194-H5N1 at the same timepoint ($p < 0.01$) (Figure 3F), suggesting a clear difference between the degree of immune dysregulation in the lungs between Cattle-H5N1 and VNM1194-H5N1.

Cattle-H5N1 shows broader tissue tropism and has a higher viral load on mammary gland tissues than VNM1194-H5N1

A prior investigation documented the presence of the HPAI A(H5N1) Clade 2.3.4.4b virus within the mammary gland of domestic dairy cattle [13]. Our study aimed to investigate further the infectivity of both Cattle-H5N1 and VNM1194-H5N1 viruses in the mammary glands of lactating BALB/c mice. Similar to the lung tissues, we detected higher $TCID_{50}$ titre and M gene copies of Cattle-H5N1 in both lactating and non-lactating mammary gland tissues at 4 dpi than VNM1194-H5N1 ($p < 0.05$), despite both viruses exhibiting low viral titres at 1 dpi (Figure 4A, Figure S8A).

Histological examination revealed pronounced tissue destruction in the mammary glands of lactating mice infected with Cattle-H5N1, manifesting as sloughing and necrosis of glandular alveolar cells (Figure 4B). This type of tissue damage was not observed in lactating mice infected with VNM1194-H5N1, which exhibited a histological profile similar to mock-infected mice except for a few alveolar cells sloughing in one or two glandular lobes. IF staining demonstrated a frequent presence of Cattle-H5N1 nucleoprotein (NP) antigen within the glandular epithelium (Figure 4C) at 4 dpi, with more prominent NP antigens in adipose tissue and lymphoid tissue attaching to the mammary gland of lactating mice (Figure S7). In contrast, only a few small foci of

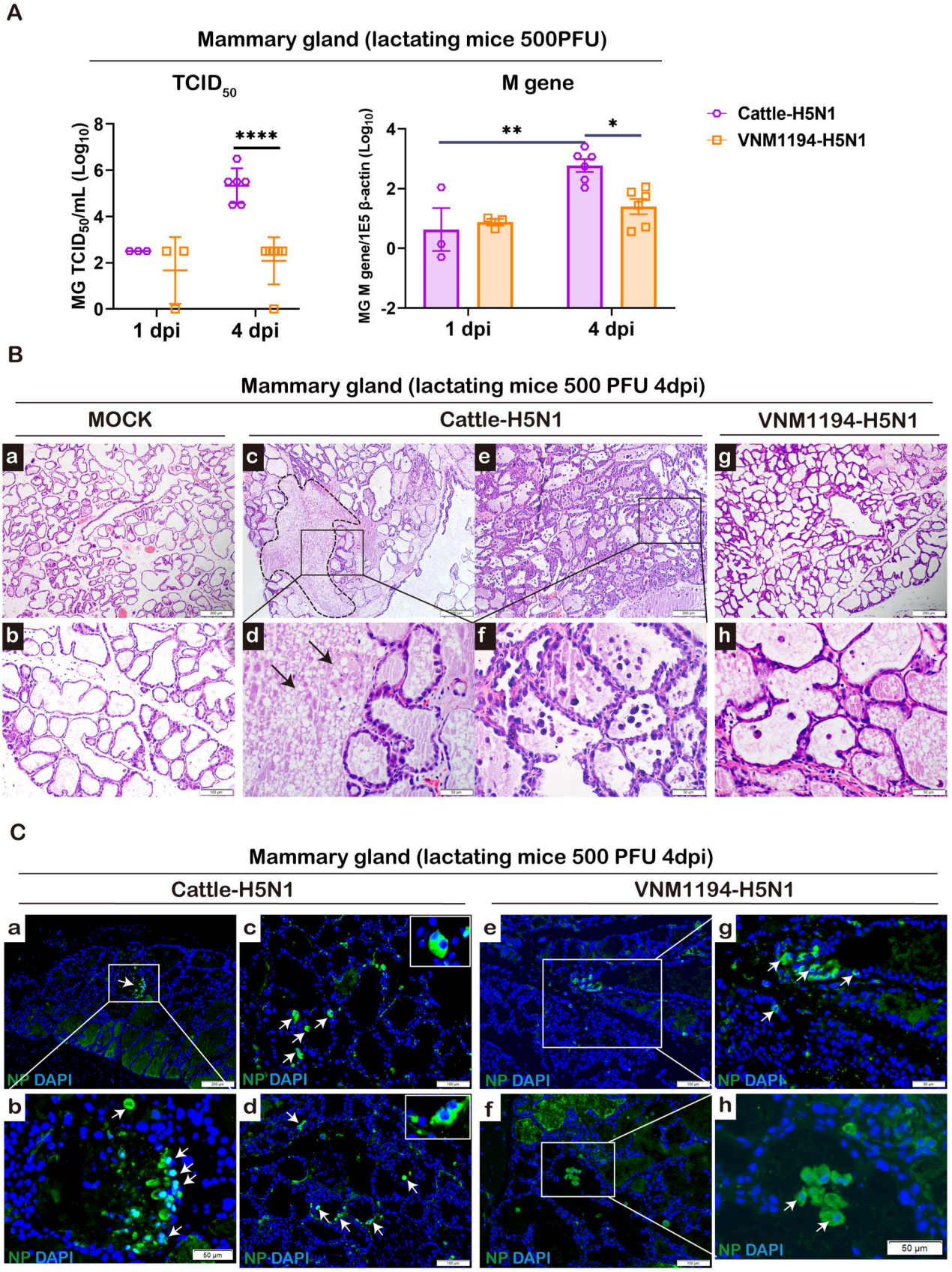

Figure 4. Viral load and histopathological changes in mammary glands of lactating BALB/c mice after infection. A. Viral loads in mammary glands of lactating BALB/c mice at 1 and 4 dpi were determined using $TCID_{50}$ assay and viral M gene copy numbers. Data were shown as mean ± SD from three or six replicates (n = 3 for 1 dpi data and n = 6 for 4 dpi data), where * $p < 0.05$, ** $p < 0.01$, **** $p < 0.0001$ were determined by Two-way ANOVA with Tukey's multiple comparisons test. B. Representative histological images (H&E-stained) of mock and infected lactating mammary gland tissues at 4 dpi. The dotted lines and black arrows indicate the "ghost structure" of necrosis. C. Representative histological images (IF-stained with anti-NP) of Cattle-H5N1 and VNM1194-H5N1 infected lactating mammary gland tissues highlighting the glandular epithelium at 4 dpi. White arrows indicate NP-positive cells. Scale bar = 50μm, 100μm or 200μm.

alveolar cells showed NP antigen expression in VNM1194-H5N1-infected mice (Figure 4C). The absence of tissue damage in VNM1194-H5N1-infected lactating mice correlated with the markedly lower NP antigen detection frequency than Cattle-H5N1.

The non-lactating mammary gland showed no visible tissue damage or inflammatory changes in Cattle-H5N1- or VNM1194-H5N1-infected mice compared to mock-infected mice (Figure S8B). Even though NP-positive cells were frequently found in the adipose part of breast tissue as diffusely distributed large foci and lymphoid tissue, NP-positive cells were rarely observed in the glandular epithelium (Figure S8B). The massive infection of adipose tissue by Cattle-H5N1 may explain why non-lactating mice infected by this virus have a high viral load in the mammary glands. The above findings demonstrated that the Cattle-H5N1 virus had a broader cell tropism for mammary gland tissues in lactating BALB/c mice, triggering significant tissue damage.

Apart from the mammary gland, we also collected transmission data from suckling mice co-housed with infected lactating mice (mother). In this study, seven lactating mice (mother) were infected with 500 PFU of Cattle-H5N1 and co-housed with three or six pups for four days before being euthanised for analysis (6–7 cages). As mentioned, all Cattle-H5N1-infected lactating mice exhibited higher viral loads, infectious titers in their mammary glands, and significant tissue damage and viral antigen expression in glandular alveolar cells than VNM1194-H5N1. Whether this observation translates to potential milk transmission remains in question, given that we managed to detect 7 out of 30 co-housed pups being infected by Cattle-H5N1, specifically in their lungs, brains, or intestines (Table S4), with the highest positive rate at 50% in cage 1 (3/6 pups infected). In comparison, only 2 out of 24 co-housed pups were infected with VNM1194-H5N1.

Cattle-H5N1 infects and replicates more effectively in the brain than VNM1194-H5N1

Previous studies have shown that VNM1194-H5N1 is neurotropic [30, 31]. In the 4-day infection course of 500 PFU infection, no clinical neurological disease signs were observed from Cattle-H5N1 or VNM1194-H5N1 infected mice, while viral genes and antigens were detected. $TCID_{50}$ titre and M gene copies in Cattle-H5N1-infected brains were significantly higher than VNM1194-H5N1 (Figure 5A). Cattle-H5N1 NP-positive cells present as clusters or foci on different anatomical regions of the brain, including the olfactory bulb, cerebral cortex, midbrain, hippocampus and cerebellum at 4 dpi, but VNM1194-H5N1 NP signals were rarely seen in the whole brain (Figure 5C and D). After 20 PFU inoculation, we observed neurological symptoms at 5 dpi, with the mice spinning their bodies, imbalanced body posture, and occasionally paralyzed limbs in 3/5 Cattle-H5N1-infected mice. In contrast, none of these disease signs was observed in 20 PFU VNM1194-H5N1 infected mice.

In the brain sections, viral antigen expression at 4 dpi of 20 PFU was at the same level as 500 PFU Cattle-H5N1 inoculation (Figure 5B), with viral-positive cells found across the whole brain, including the olfactory bulb, cerebellum, hippocampus, midbrain, and cerebral cortex. The intensity and frequency of viral antigen-expressing cells increased drastically at 7 dpi (Figure 5E); notably, the ventricle membrane and choroid plexus were massively involved by virus infection, with ependymal cell death easily seen. H&E-stained brain sections showed no observable tissue damage or inflammatory change at 4 dpi in either 500 PFU or 20 PFU infection. However, inflammatory changes, including vessel congestion, perivascular immune cell accumulation, foci of haemorrhage, immune infiltration of the meningeal membrane, and ventricle membrane, could easily be observed at 7 dpi after 20 PFU infection with Cattle-H5N1 (Figure 5F). In contrast, only sparse viral antigen-positive cells, blood vessel congestion, and mild immune cell accumulation around blood vessels were seen at 7 dpi in the VNM1194-H5N1 infected mouse brain (Figure 5E and F).

Cattle-H5N1 disseminates widely and replicates more effectively in extrapulmonary organs and tissues than VNM1194-H5N1, contributing to systemic immune dysregulation

To assess and compare the systemic spread of Cattle-H5N1 and VNM1194-H5N1, we examined their presence and scope of viral RNA and antigen in whole blood, eyes, heart, thoracic cavity adipose tissue, thymus, intestine and spleen collected at 4 dpi. We observed significantly higher $TCID_{50}$ titre and M gene copies in Cattle-H5N1-infected eyes than VNM1194-H5N1 (Figure S9). Interestingly, there were substantially higher $TCID_{50}$ and M gene copies of VNM1194-H5N1 in the intestine tissues at 4 dpi compared to Cattle-H5N1. In addition, Cattle-H5N1-infected mice had higher M gene copies in whole blood specimens than VNM1194-H1N1 (Figure S9).

Next, we performed IHC and IF staining of viral NP antigens in different tissues. Several large foci of Cattle-H5N1 NP-positive cardiomyocytes were observed in the heart, but not for VNM1194-H5N1 (Figure S10A). In addition, NP-positive cells were found in the eye, muscle, thymus and thoracic fat of cattle-H5N1 infected mice (Figure S10B). We also

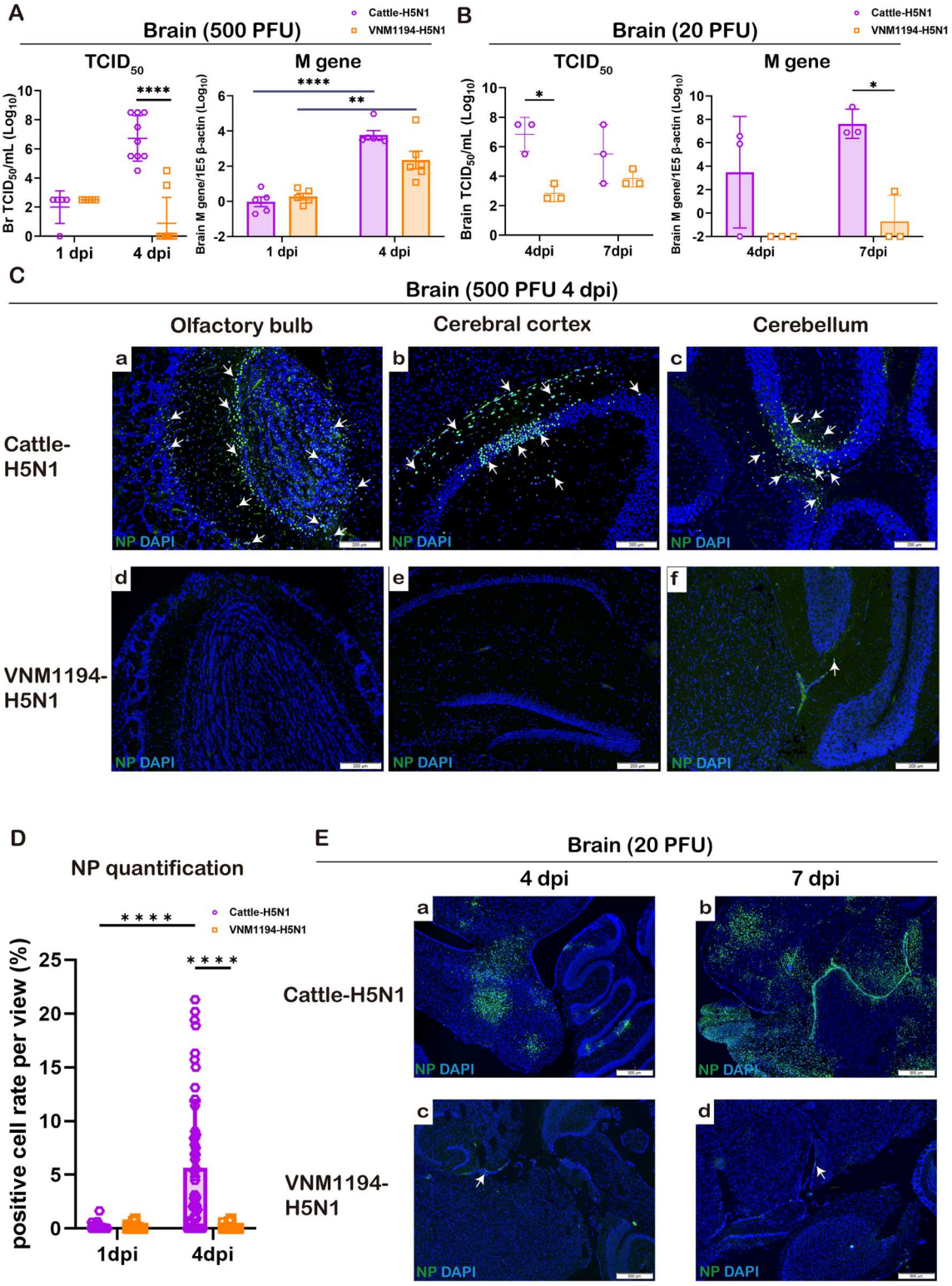

Figure 5. Viral dissemination in the brain of BALB/c mice. A. Viral loads in the brain at 1 and 4 dpi were determined using $TCID_{50}$ assay and/or viral M gene copy numbers. Data were shown as mean ± SD (n = 5 for 1dpi data, n = 6 for 4 dpi PCR data, and n = 9 for 4 dpi $TCID_{50}$ data), where ** $p < 0.01$, **** $p < 0.0001$ were determined by Two-way ANOVA with Tukey's multiple comparisons test. B. Viral loads in the brain at 4 and 7dpi were determined by $TCID_{50}$ assay and viral M gene copy numbers in tissue homogenates. Data were shown as mean ± SD (n = 3), where * $p < 0.05$ were determined by Two-way ANOVA with Tukey's multiple comparisons test. C. Representative IF-stained with anti-NP images of Cattle-H5N1 and VNM1194-H5N1 infected brain tissue sections at 4 dpi. White arrows indicate NP-positive cells. Scale bar = 200μm. D. NP quantification of infected brain at 1 and 4 dpi. Data were shown as mean ± SD (n = 50), where **** $p < 0.0001$ were determined by Two-way ANOVA with Tukey's multiple comparisons test. E. Representative IF-stained with anti-NP images of Cattle-H5N1 and VNM1194-H5N1 infected brain tissue sections at 4 and 7dpi. White arrows indicate NP-positive cells. Scale bar = 500μm. F. Representative H&E images of Cattle-H5N1 and VNM1194-H5N1 infected brain tissue sections at 7 dpi. Black arrows indicate the immune cell infiltration in the ventricle or meninge with meningeal vessel congestion. Green arrows indicate the dead and detached ependymal cells in the choroid plexus. White arrows indicate the immune cell accumulating around the blood vessel. Red arrows indicate the haemorrhage foci in the Cattle-H5N1 infected brain, while these haemorrhage foci were not seen in the VNM1194-H5N1 infected brain. Scale bar = 100 or 200μm.

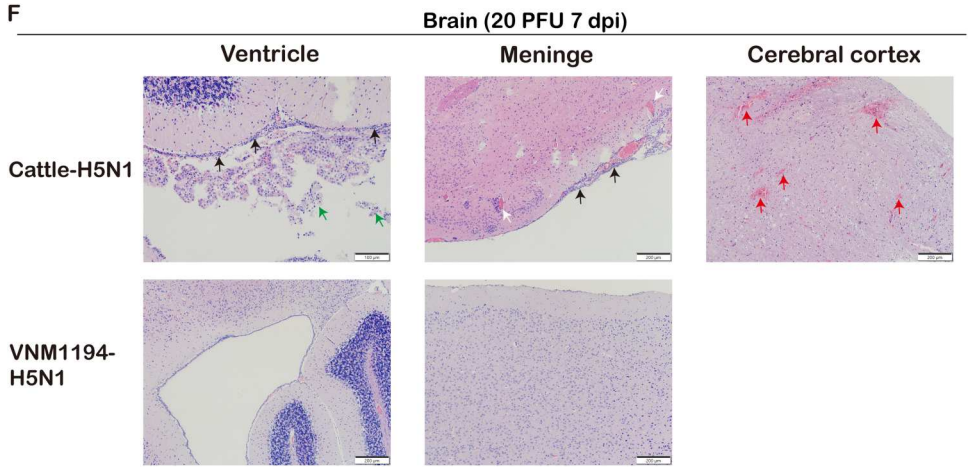

Figure 5. *Continued*

found that the mouse spleen is another crucial extra-pulmonary organ heavily infected by the Cattle-H5N1 virus. NP-positive cells in Cattle-H5N1-infected spleen were observably much more frequent than in VNM1194-H5N1-infected mice (Figure 6A and S11B). Our observation in the spleen was further confirmed by the quantitation of NP-positive cells by flow cytometry, which showed that the Cattle-H5N1 infection had a significantly higher percentage (5.3%) of NP-positive than VNM1194-H5N1 (0.7%) when gated by CD45 as total splenocytes (Figure 6C). Among different cell types, $B220^+$ B cells (7.01%), Dendritic cells (DC) (10.9%), and monocytes (17.3%) showed significantly higher frequency to be NP positive compared to VNM1194-H5N1 infected mouse spleen, with 3.48%, 2.6%, and 0.4% for B cells, DC, and monocytes, respectively ($p < 0.05$), while only the difference in the percentage of NP positive $CD3^+$ T cells was less significant (3.418% vs 2.358%, $p = 0.284$) (Figure 6C). Histologically, prominent splenocyte atrophy and foci of death cell debris were readily seen in the Cattle-H5N1 spleen sections, which was further supported by drastically increased TUNEL labelled apoptotic cells and decreased anti-B220 and anti-CD3 labelled B cell or T cells respectively (Figure 6A and B). At the same time, these histopathological signs were occasionally observed in VNM1194-H5N1 (Figure S11B). These observations implied that Cattle-H5N1 could infect more splenocytes, which may contribute to a more significant impairment of the immune responses than VNM1194-H5N1 during the later stages of infection and cause a significant drop in the survival rate in Cattle-H5N1-infected mice at 500 PFU (Figure 1D).

Concurrently, given the higher NP positive and apoptosis of Cattle-H5N1-infected splenocytes compared to VNM1194-H5N1, we also aim to determine whether there is a difference in the expression of pro-inflammatory cytokines in the serum. The infected mice sera were collected at 1 and 4 dpi and were tested for cytokine/chemokine concentration using the LEGENDplex^{TM} bead-based cytokine immunoassay. At 1 dpi, both Cattle-H5N1 and VNM1194-H5N1 infection did not induce a detectable increase of serum cytokine responses, except for CXCL10, which is significantly induced by VNM1194-H5N1 compared to mock ($p < 0.05$) (Figure 6D). In contrast, the increase was insignificant in Cattle-H5N1 ($p = 0.2073$). At 4 dpi, the serum of Cattle-H5N1-infected mice exhibited significantly elevated protein levels of IFN-α, IFN-γ, TNF-α, IL-6, CCL2, CCL4, CXCL9, and CXCL10 compared to VNM1194-H5N1 infection ($p < 0.05$), concurring with the levels observed in the Cattle-H5N1-infected lung tissues. Increased aberration of cytokine/chemokine expression in the serum from Cattle-H5N1 could lead to hyperinflammation, allowing Cattle-H5N1 to cause more systemic multi-organ dysfunction than VNM1194-H5N1.

Discussion

The detection of HPAI H5N1 Clade 2.3.4.4b genotype B3.13 virus in lactating dairy cattle in March 2024, with the virus found in milk and nasal swabs, has raised concerns beyond the immediate health of dairy cattle [13]. The potential for zoonotic spill-over to the human population is a significant concern, especially considering the high viral loads found in unpasteurized milk, which increases the risk for farm workers in close contact with infected animals and milking equipment [32]. The virus likely emerged in late 2023 [18] and has evolved considerably from A/Vietnam/1194/2004 (VNM1194-H5N1), which belonged to Clade 1 in 2004 and has previously been developed as a pre-pandemic candidate influenza vaccine [33]. More recently, phylogenetic analyzes of the HA and NA genes of the Cattle-H5N1 virus revealed that it evolved from A/Texas/37/2024 [14] and formed a cluster with recently reported H5N1 isolates from

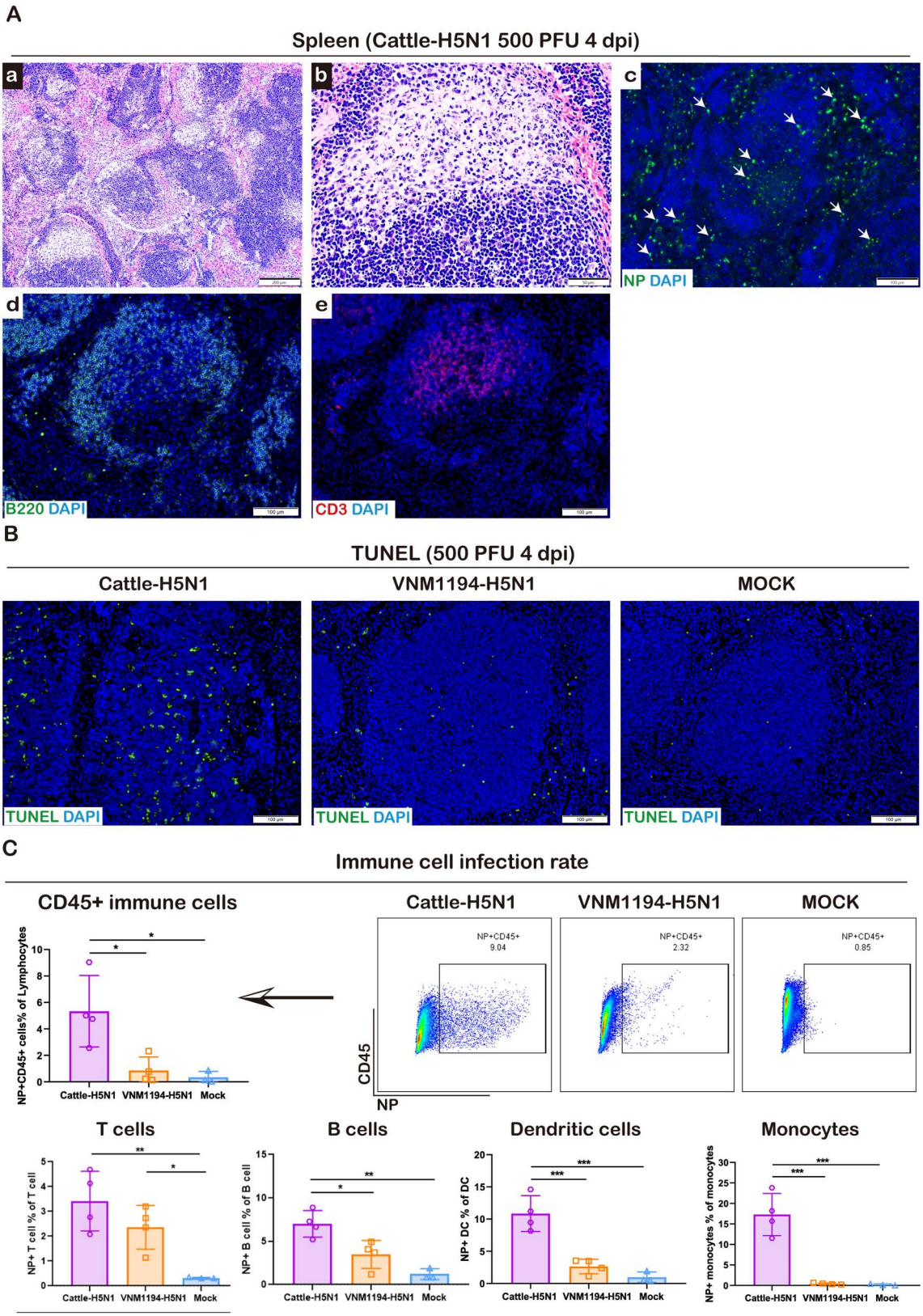

Figure 6. Histopathological changes and immunological profiles in the spleen of BALB/c mice after infection. A. Representative histological images (H&E-stained, IF-stained with anti-NP, anti-B220, and anti-CD3-stained) of Cattle-H5N1 infected spleen tissue sections at 4 dpi. White arrows indicate NP-positive cells. Mock and VNM1194-H5N1 infected spleen tissues are shown in Figure S11. B. Representative TUNEL-stained histological images of infected spleen tissue sections at 4 dpi. Scale bar = 100μm or 200μm. C. Percentage of NP^+ $CD45^+$ leukocytes, NP^+ $CD45^+$ $B220^+$ B cells, NP^+ $CD45^+$ $CD3^+$ T cells, NP^+ Dendritic cells, and NP^+ monocytes in the spleen tissues by flow cytometry analysis after infection at 4 dpi. Data were shown as mean ± SD from three or four replicates (n = 3 for the mock group and n = 4 for the infection group), where * $p < 0.05$, ** $p < 0.01$, *** $p < 0.001$ were determined by One-way ANOVA with Tukey's multiple comparisons test. D. Selected cytokine and chemokine protein levels at 1 and 4 dpi presented in serum. Data were shown as mean ± SD from three or five replicates (n = 3 for the mock group and n = 5 for the infection group), where * $p < 0.05$, ** $p < 0.01$, *** $p < 0.001$, **** $p < 0.0001$ were determined by One-way ANOVA with Tukey's multiple comparisons test.

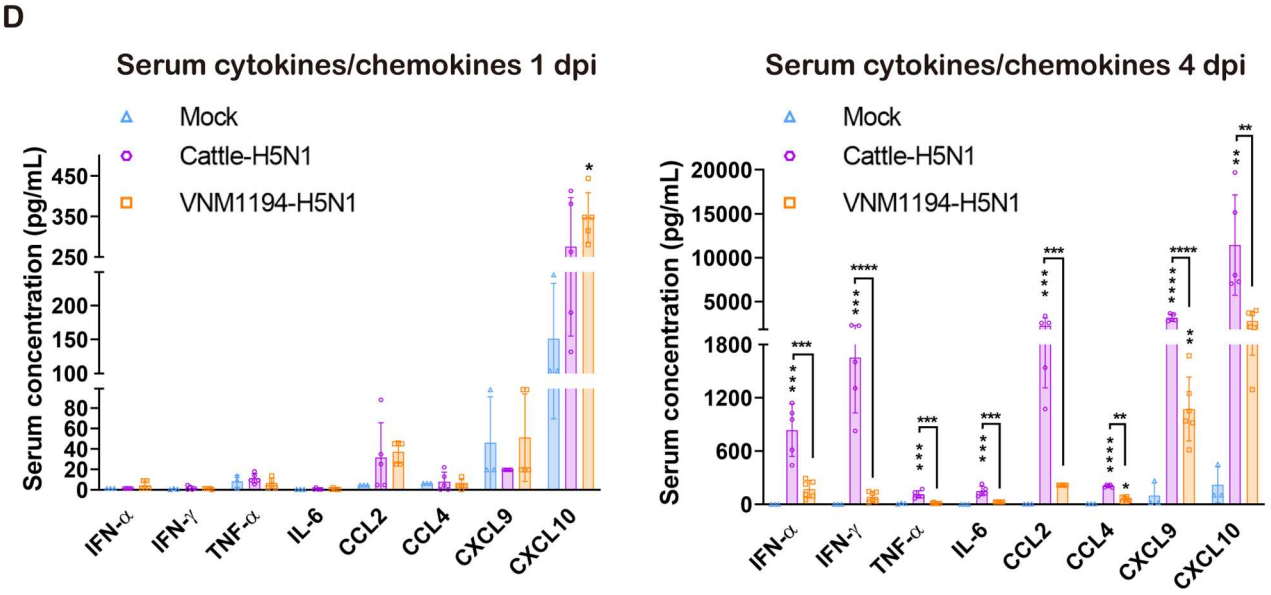

Figure 6. *Continued*

humans, cats, and cows (namely Texas/37-like cluster), which belonged to genotype B3.13 [18]. This genotype emerged from a reassortment event between genotype B3.7 (contributing the PB2, PB1, PA, HA, NA, M, and NS genes) and a low pathogenic avian influenza (LPAI) virus – H11N9 (contributing NP gene) [18]. The virus's ability to adapt and spread efficiently among mammals underscores the need to evaluate its pathogenicity in various mammalian animals. In this investigation, we inoculated female BALB/c mice with A/dairy cattle/Texas/24-008749-003/2024 (Cattle-H5N1) virus. We found that this H5N1 virus is well adapted for mice (without the need for multiple passages or prior adaptation); it infects and replicates at a much higher efficiency in the airway and lung than the older H5N1 virus, VNM1194-H5N1. After intranasal infection, the Cattle-H5N1 virus disseminates quickly through the body, replicating in multiple organs, resulting in severe tissue destruction and dysregulated immune responses. Except for changes in the mammary gland in lactating mice, there are no differences in the histopathological changes between lactating and non-lactating mice.

In vitro, Cattle-H5N1 infection of human respiratory cell lines, A549 and Calu-3, had a higher replication rate in cell lines compared to VNM1194-H5N1. The higher replication rate of Cattle-H5N1 may also allow more widespread systemic dissemination across the lung and extrapulmonary organs in BALB/c mice than VNM1194-H5N1 at 4 dpi, characterized by more significant lesions and intensive viral NP antigen expression in the lungs, mammary glands, brain, eye, intestine, heart, whole blood, and spleen tissues. Although previous studies observed lesions in the lung and mammary gland tissues after the Cattle-H5N1-like virus infected dairy cows and domestic cats [13, 34], these studies did not compare the histopathological profile of this virus to an older H5N1. Furthermore, a recent report that compared the pathogenicity of A/dairy cattle/New Mexico/A240920343-93/2024 and A/Vietnam/1203/2004 in BALB/c mice did not observe any notable differences in terms of viral load or dissemination in pulmonary and extrapulmonary organs, which might be due to the high initial PFU (10^3 PFU) used for intranasal inoculation that results in 0% survival rate in 8 dpi [15]. In this study, we used a high and lower PFU of 500 and 20, and we were able to observe a significant difference in viral titre and distinct viral dissemination patterns in various organs at 4 dpi between Cattle-H5N1 and VNM1194-H5N1, which confirms that Cattle-H5N1 is more adapted to the mammalian system.

The difference in systemic manifestations could be attributed to the differences in the genetic makeup of these two viruses. When we analyzed the amino acid substitutions arising from nonsynonymous mutations between Cattle-H5N1 and VNM1194-H5N1 (Figure 1A, Table S3), we identified notable substitutions previously reported to be associated with increased pathogenicity/virulence, transmission and adaptation in mammals [35], such as K156A in the receptor binding domain of the HA protein [36, 37] and N205S in the effector domain of NS1 which was found to be able to enhance polymerase function if phosphorylation occurs on this site [38], Additionally, three structural differences exhibited between these two viruses are the HA polybasic cleavage site, NA stalk region, and NS1 linker region (Figure 1A), which could be critical molecular determinants of their distinct virulence. The VNM1194-H5N1 virus,

which harbors the RRRKKR↓G HA polybasic cleavage site, was previously assessed for its role in contributing to pathogenicity and neurovirulence in BALB/c mice and was found to be less potent compared to SRRKKR↓G [39]. However, to our knowledge, the virulence of KRRKR↓G harbored by the Cattle-H5N1 has yet to be assessed [40]. Furthermore, the long NA stalk length (characterized by the 20 amino acid motifs present in Cattle-H5N1) was previously considered less virulent in mice than the short stalk length [41]. Still, the longer NA stalk length may be preferentially paired with the H5 with fewer glycosylation sites to increase virus fitness and spread to diverse species [42]. Lastly, the five amino acid insertion in the NS1 linker domain (present in Cattle-H5N1) was previously found to enhance pathogenicity in BALB/c mice and increase expression of IL-6, MX1 and CXCL10 in their lungs [43]. Besides insertions in the HA, NA, and NS1 of Cattle-H5N1, amino acid substitutions in the polymerase complex proteins, such as on the PA protein (K497R) and PB2 protein (M631L), may further enhance Cattle-H5N1's polymerase activity (Table S3), which could result in increasing virus replication and severity of infection in mice [44, 45]. These notable features, which are present in Cattle-H5N1 but not in VNM1194-H5N1 (Figure 1A, Table S3), are likely to be the virulence factors that elevate the Cattle-H5N1 pathogenicity in BALB/c mice, but their specific role in interacting/hijacking host factors and whether these virulence factors also increase Cattle-H5N1 pathogenicity in other mammalian models such as hamsters requires further investigation.

The distinct amino acid substitutions at the HA surface glycoprotein between Cattle-H5N1 and VNM1194-H5N1 could be implicated in their difference in receptor-binding specificity between these two viruses; hence, the increased extrapulmonary infectivity acquired by Cattle-H5N1. As previously reported, Cattle-H5N1-like viruses were found to display both human- and avian-type receptor-binding properties [15] by binding to α2,6-linked sialic acids (preferred by human influenza) and α2,3-linked sialic acids (preferred by avian influenza). The increase of the receptor binding breath could be due to a single mutation, T211I (or T199I, H3 numbering), at the receptor binding site of HA [46], thus allowing Cattle-H5N1 to infect either the lactating or non-lactating mammary tissues rich in both α2,3-linked and α2,6-linked sialic acids [47, 48]. However, there is still no direct evidence that the dual receptor usage of Cattle-H5N1 increases its infectivity in extrapulmonary tissue, which requires further investigation. Interestingly, we also found NP-positive cell clusters in the olfactory bulb, cerebral cortex, and cerebellum of the Cattle-H5N1-infected brain at 4 dpi but not for VNM1194-H5N1 infection, which concurs with the previous observation that VNM1194-H5N1 has reduced neurotropism in mice [30]. The Cattle-H5N1-infected cell clusters in each structure preferentially appear in the granular layer that depends on an extensive capillary network to deliver oxygen and nutrients and remove metabolic waste, which suggests that this virus has enhanced ability to breach the blood–brain barrier due to better neuroinvasiveness. Intriguingly, although the neuroinvasion of Cattle-H5N1 in the mice's brain was likely due to its efficient replication starting in the olfactory mucosa as well as the presence of α2,3- and α2,6-linked sialic acids in the olfactory bulb/cerebral cortex/cerebellum, which was a notable feature of several HPAI H5Nx, we did not observe signs of neurovirulence at our post-infection timepoint (4 dpi) for both Cattle-H5N1 and VNM1194-H5N1. A closely related VNM1194-H5N1 virus, such as A/Vietnam/1203/2004, was previously known to induce neuroinflammation and neurodegeneration in C57BL/6J mice, but significant loss of neurons and increase of inflammatory response could only be observed around 60–90 dpi. This suggests that Cattle-H5N1 could also induce neurodegenerative pathologies, provided that a sublethal intranasal inoculation dose is used and the mice model survives the acute infection but retains long-term neurologic consequences of H5N1 infection [49, 50].

One peculiar observation in our current study about the pathogenicity of Cattle-H5N1 and VNM1194-H5N1 was the immune response in the lungs of infected BALB/c mice. Firstly, the discrepancy between protein and mRNA levels of cytokines/chemokines in Cattle-H5N1 and VNM1194-H5N1 infected lungs (Figure 3E and F) suggests that Cattle-H5N1, with the aid of its immune antagonist NS1 [51], could be more effective in blocking signaling pathways that activate the transcription of genes expressing or are involved in cytokine, chemokine, and ISG production during its replication, thus showing lower mRNA levels than VNM1194-H5N1. However, the higher protein levels of cytokines/chemokines could also be due to the ability of Cattle-H5N1 to produce a higher amount of defective viral genomes (DVGs) or mini viral RNAs (mvRNAs) at 4 dpi, which stimulates a more robust antiviral response and cytokine induction [52, 53]. Nonetheless, among all chemokines investigated in this study, the chemokine CXCL10 (C-X-C motif chemokine ligand 10, also known as interferon-gamma-induced protein 10 or IP-10) in the lungs and serum, showed the highest levels at 4 dpi after Cattle-H5N1 infection and was considerably higher than VNM1194-H5N1 in the serum ($p < 0.01$). Despite the elevated levels of CXCL10 and other chemokines in Cattle-H5N1-infected lungs/serum, which was known to facilitate chemoattraction of lymphocytes (such as T cells and Natural Killer cells), immune

cell accumulation in the lungs was not evident at 4 dpi (Figure 3A). Together with the broader cell tropism and extrapulmonary spread of Cattle-H5N1, this suggests a lack of early control by innate immunity compared to VNM1194-H5N1. Another reason could be the severe cellular destruction and impaired production of monocytes and lymphocytes (such as T cells) in the spleen due to severe infection by Cattle-H5N1, as evident by the widespread TUNEL positivity and degeneration or atrophy of spleen follicles. The Cattle-H5N1's ability to cause more pronounced systemic infection may also lead to heightened stimulation of T cells in the lymphoid organs [54], contributing to early exhaustion of T cell response and exacerbating their lower circulation in the lungs.

In this study, we only found one milk sample positive with Cattle-H5N1 from a lactating mother of BALB/c mice after being intranasally inoculated with 20 PFU at 7 dpi (figure not presented), which could be due to the significant mammary gland tissue damage caused by the virus resulting in substantial loss of milk product. This phenomenon was also seen in the mammary glands of H5N1-infected dairy cows [55]. Given the lack of virus-positive milk samples in our study, we did not perform oral inoculation on the lactating mother as previous studies have already established that oral inoculation of cow milk with high H5N1 titer in the mice caused respiratory infection [15, 56]. Still, oral (milk) transmission has not yet been established as the primary route for Cattle-H5N1 in the actual transmission settings among cows. Hence, we performed intranasal inoculation on the lactating mother to assess the potential transmission between lactating mothers and pups. We managed to detect the Cattle-H5N1 M gene (by RT-qPCR) in 7/30 co-housed pup's lung, brain, and intestine samples after 4 dpi, suggesting that "secondary and vertical" milk transmission (through the oral route) is still possible (apart from the conventional airborne transmission) between lactating mothers and pups, despite the shorter period of post-infection and the limited Cattle-H5N1 positive in the milk of lactating mice. Our results concurred with the observation reported by Eisfeld et al. (2024), who found that not every lactating mice had milk positively detected for the virus after intranasal inoculation (0/6 at 4 dpi; 2/9 at 7 dpi; 3/6 at 9 dpi), yet less than one-third of the co-housed pups had acquired infection from lactating mother (0/25 pups at 4 dpi; 4/24 at 7 dpi; 11/30 at 9 dpi) [15]. The lethality dose of Cattle-H5N1, which permits both prolonged infection and presence in milk and increases the virus's ability to induce long-term neurovirulence symptoms at more extended post-infection or post-recovery periods in the mice model, requires further investigation [15, 49, 50].

In conclusion, our current study underscores the potential for widespread systemic infection of a terrestrial mammalian-adapted HPAI H5N1 virus in a BALB/c mice model infected by intranasal challenge. One limitation of our study is the lack of pathological comparison between H5N1 Clade 2.3.4.4b viruses of more recent strains (e.g. genotype B3.13) or different animal origins. But we chose an older Clade 1 virus (VNM1194-H5N1) for comparison, given that the pathological features of this virus were well described in mice and other animal models previously [19, 28], which could provide a clear baseline for pathological observation of Cattle-H5N1. Nonetheless, our findings emphasize the urgent need for further research to understand the pathogenicity and transmission routes of Cattle-H5N1 fully in other animal models, given its more enhanced systemic infection compared to VNM1194-H5N1. While the Cattle-H5N1-like viruses have caused relatively mild and typical flu-like symptoms with no fatality and human transmission reported in livestock handlers yet [57], antigenic drift could continue to occur, resulting in a more than 50% case fatality rate as exhibited by VNM1194-H5N1-like viruses previously [58]. With further genetic changes, it can be readily envisaged that a mother-to-baby transmission may occur in a mildly symptomatic mother, which leads to severe H5N1 infection in an infant with an immature immune system. Hence, close monitoring of person-to-person transmission and the evolution of the Cattle-H5N1-like virus is warranted, given its higher virulence than the Clade 1 virus in mouse models. Future research should also focus on understanding the mechanisms of pathogenicity in Cattle-H5N1 infection in different mammalian models to fully grasp its potential for various zoonotic transmission routes.

Acknowledgements

We thank our colleagues at the Centre for Comparative Medicine Research (CCMR) and Core Facility, HKU for their tremendous support.

Disclosure statement

No potential conflict of interest was reported by the author(s).

Funding

This study was partly supported by funding from Health@InnoHK, Innovation and Technology Commission, the Government of the Hong Kong Special Administrative Region; Partnership Programme of Enhancing Laboratory Surveillance and Investigation of Emerging Infectious Diseases and Antimicrobial Resistance for the Department of Health of the Hong Kong Special Administrative Region

Government; Sanming Project of Medicine in Shenzhen, China (SZSM201911014); the High Level-Hospital Program, Health Commission of Guangdong Province, China; the University of Hong Kong Outstanding Young Researcher Award; and the University of Hong Kong Research Output Prize (Li Ka Shing Faculty of Medicine); and donations from May Tam Mak Mei Yin, Richard Yu and Carol Yu, the Shaw Foundation Hong Kong, Michael Seak-Kan Tong, Lee Wan Keung Charity Foundation Limited, Providence Foundation Limited (in memory of the late Lui Hac-Minh), Hong Kong Sanatorium and Hospital, Hui Ming, Hui Hoy and Chow Sin Lan Charity Fund Limited, The Chen Wai Wai Vivien Foundation Limited, Chan Yin Chuen Memorial Charitable Foundation, Marina Man-Wai Lee, the Hong Kong Hainan Commercial Association South China Microbiology Research Fund, and Lo Ying Shek Chi Wai Foundation. The funding sources had no role in the study design, data collection, analysis, interpretation, or writing of the report.

Author contributions

NX, XYO, AJ-XZ, HLC and K-YY had roles in the study design, data collection, data analysis, data interpretation, and writing of the manuscript. YXC, CL, HH-CC, PW, ZHY AH-CL and WCS had roles in performing different experiments and data collection. AC-YL, JF-WC and SFY had roles in data interpretation and manuscript writing. All authors reviewed and approved the final version of the manuscript.

ORCID

Andrew Chak-Yiu Lee http://orcid.org/0000-0002-8432-3282
Kin-Hang Kok http://orcid.org/0000-0003-3426-332X
Shuofeng Yuan http://orcid.org/0000-0001-7996-1119
Honglin Chen http://orcid.org/0000-0001-5108-8338

References

[1] To KK, Ng KH, Que TL, et al. Avian influenza A H5N1 virus: a continuous threat to humans. Emerg Microbes Infect. 2012;1(9):1–12. doi:10.1038/emi.2012.24
[2] Garg S, Reed C, Davis CT, et al. Outbreak of highly pathogenic avian influenza A(H5N1) viruses in U.S. dairy cattle and detection of two human cases – United States, 2024. MMWR Morb Mortal Wkly Rep. 2024;73(21):501–505. doi:10.15585/mmwr.mm7321e1
[3] Cheng Vincent CC, To Kelvin KW, Tse H, et al. Two years after pandemic influenza A/2009/H1N1: what have we learned? Clin Microbiol Rev. 2012;25(2):223–263. doi:10.1128/CMR.05012-11
[4] Xu X, Subbarao K, Cox NJ, et al. Genetic characterization of the pathogenic influenza A/Goose/Guangdong/1/96 (H5N1) virus: similarity of its hemagglutinin gene to those of H5N1 viruses from the 1997 outbreaks in Hong Kong. Virology. 1999;261(1):15–19. doi:10.1006/viro.1999.9820
[5] Yuen KY, Chan PK, Peiris M, et al. Clinical features and rapid viral diagnosis of human disease associated with avian influenza A H5N1 virus. Lancet. 1998;351(9101):467–471. doi:10.1016/S0140-6736(98)01182-9
[6] Duan L, Campitelli L, Fan XH, et al. Characterization of low-pathogenic H5 subtype influenza viruses from Eurasia: implications for the origin of highly pathogenic H5N1 viruses. J Virol. 2007;81(14):7529–7539. doi:10.1128/JVI.00327-07
[7] Revised and updated nomenclature for highly pathogenic avian influenza A (H5N1) viruses. Influenza Other Respir Viruses. 2014;8(3):384–388. doi:10.1111/irv.12230
[8] Kandeil A, Patton C, Jones JC, et al. Rapid evolution of A(H5N1) influenza viruses after intercontinental spread to North America. Nat Commun. 2023;14(1):3082. doi:10.1038/s41467-023-38415-7
[9] Castro-Sanguinetti GR, González-Veliz R, Callupe-Leyva A, et al. Highly pathogenic avian influenza virus H5N1 clade 2.3.4.4b from Peru forms a monophyletic group with Chilean isolates in South America. Sci Rep. 2024;14(1):3635. doi:10.1038/s41598-024-54072-2
[10] Elsmo EJ, Wünschmann A, Beckmen KB, et al. Highly pathogenic avian influenza A(H5N1) virus Clade 2.3.4.4b infections in wild terrestrial mammals, United States, 2022. Emerg Infect Dis. 2023;29(12):2451–2460. doi:10.3201/eid2912.230464
[11] Agüero M, Monne I, Sánchez A, et al. Highly pathogenic avian influenza A(H5N1) virus infection in farmed minks, Spain, October 2022. Eurosurveillance. 2023;28(3):2300001. doi:10.2807/1560-7917.ES.2023.28.3.2300001
[12] Leguia M, Garcia-Glaessner A, Muñoz-Saavedra B, et al. Highly pathogenic avian influenza A(H5N1) in marine mammals and seabirds in Peru. Nat Commun. 2023;14(1):5489. doi:10.1038/s41467-023-41182-0
[13] Burrough ER, Magstadt DR, Petersen B, et al. Highly pathogenic avian influenza A(H5N1) Clade 2.3.4.4b virus infection in domestic dairy cattle and cats, United States, 2024. Emerg Infect Dis. 2024;30(7):1335–1343. doi:10.3201/eid3007.240508
[14] Uyeki TM, Milton S, Abdul Hamid C, et al. Highly pathogenic avian influenza A(H5N1) virus infection in a dairy farm worker. N Engl J Med. 2024;390(21):2028–2029. doi:10.1056/NEJMc2405371
[15] Eisfeld AJ, Biswas A, Guan L, et al. Pathogenicity and transmissibility of bovine H5N1 influenza virus. Nature. 2024;633(8029):426–432. doi:10.1038/s41586-024-07766-6
[16] Belshe RB, Frey SE, Graham I, et al. Safety and immunogenicity of influenza A H5 subunit vaccines: effect of vaccine schedule and antigenic variant. J Infect Dis. 2011;203(5):666–673. doi:10.1093/infdis/jiq093
[17] Lu X, Tumpey TM, Morken T, et al. A mouse model for the evaluation of pathogenesis and immunity to influenza A (H5N1) viruses isolated from humans. J Virol. 1999;73(7):5903–5911. doi:10.1128/JVI.73.7.5903-5911.1999
[18] Hu X, Saxena A, Magstadt DR, et al. Genomic characterization of highly pathogenic avian influenza A H5N1 virus newly emerged in dairy cattle. Emerging Microbes Infect. 2024;13(1):2380421. doi:10.1080/22221751.2024.2380421
[19] Zheng BJ, Chan KW, Lin YP, et al. Delayed antiviral plus immunomodulator treatment still reduces

mortality in mice infected by high inoculum of influenza A/H5N1 virus. Proc Natl Acad Sci USA. 2008;105(23):8091–8096. doi:10.1073/pnas.0711942105

[20] Li IW, Chan KH, To KW, et al. Differential susceptibility of different cell lines to swine-origin influenza A H1N1, seasonal human influenza A H1N1, and avian influenza A H5N1 viruses. J Clin Virol. 2009;46(4):325–330. doi:10.1016/j.jcv.2009.09.013

[21] Li C, Li C, Zhang AJ, et al. Avian influenza A H7N9 virus induces severe pneumonia in mice without prior adaptation and responds to a combination of zanamivir and COX-2 inhibitor. PLoS One. 2014;9(9):e107966. doi:10.1371/journal.pone.0107966

[22] Li C, Ye Z, Zhang AJX, et al. Severe acute respiratory syndrome coronavirus 2 (SARS-CoV-2) infection by intranasal or intratesticular route induces testicular damage. Clin Infect Dis. 2022;75(1):e974–ee90. doi:10.1093/cid/ciac142

[23] Reed LJ, Muench H. (1938). A simple method of estimating fifty per cent endpoints.

[24] Lee AC, Zhang AJ, Chan JF, et al. Oral SARS-CoV-2 inoculation establishes subclinical respiratory infection with virus shedding in golden Syrian hamsters. Cell Rep Med. 2020;1(7):100121. doi:10.1016/j.xcrm.2020.100121

[25] Livak KJ, Schmittgen TD. Analysis of relative gene expression data using real-time quantitative PCR and the 2− ΔΔCT method. Methods. 2001;25(4):402–408. doi:10.1006/meth.2001.1262

[26] Ghasemi A, Zahediasl S. Normality tests for statistical analysis: a guide for non-statisticians. Int J Endocrinol Metab. 2012;10(2):486–489. doi:10.5812/ijem.3505

[27] Guan L, Eisfeld AJ, Pattinson D, et al. Cow's milk containing avian influenza A(H5N1) virus—heat inactivation and infectivity in mice. N Engl J Med. 2024;391(1):87–90. doi:10.1056/NEJMc2405495

[28] Lee AC-Y, Zhang AJ, Li C, et al. Intradermal vaccination of live attenuated influenza vaccine protects mice against homologous and heterologous influenza challenges. npj Vaccines. 2021;6(1):95. doi:10.1038/s41541-021-00359-8

[29] Kao RY, Yang D, Lau LS, et al. Identification of influenza A nucleoprotein as an antiviral target. Nat Biotechnol. 2010;28(6):600–605. doi:10.1038/nbt.1638

[30] Li J, Liu B, Chang G, et al. Virulence of H5N1 virus in mice attenuates after in vitro serial passages. Virol J. 2011;8:93. doi:10.1186/1743-422X-8-93

[31] Bauer L, Benavides FF, Kroeze EJV, et al. The neuropathogenesis of highly pathogenic avian influenza H5Nx viruses in mammalian species including humans. Trends Neurosci. 2023;46(11):953–970. doi:10.1016/j.tins.2023.08.002

[32] Le Sage V, Campbell A, Reed DS, et al. Persistence of influenza H5N1 and H1N1 viruses in unpasteurized milk on milking unit surfaces. Emerg Infect Dis. 2024;30(8):1721–1723. doi: 10.3201/eid3008.240775

[33] Díez-Domingo J, Garcés-Sanchez M, Baldó JM, et al. Immunogenicity and Safety of H5N1 A/Vietnam/1194/2004 (Clade 1) AS03-adjuvanted prepandemic candidate influenza vaccines in children aged 3 to 9 years: a phase ii, randomized, open, controlled study. Pediatr Infect Dis J. 2010;29(6):e35–e46. doi:10.1097/INF.0b013e3181daf921

[34] Baker AL, Arruda B, Palmer MV, et al. Experimental reproduction of viral replication and disease in dairy calves and lactating cows inoculated with highly pathogenic avian influenza H5N1 clade 2.3. 4.4 b. bioRxiv. 2024:2024.07.12.603337.

[35] Nguyen TQ, Hutter C, Markin A, et al. Emergence and interstate spread of highly pathogenic avian influenza A (H5N1) in dairy cattle. bioRxiv. 2024:2024.05.01.591751.

[36] Linster M, van Boheemen S, de Graaf M, et al. Identification, characterization, and natural selection of mutations driving airborne transmission of A/H5N1 virus. Cell. 2014;157(2):329–339. doi:10.1016/j.cell.2014.02.040

[37] Antigua KJC, Baek YH, Choi WS, et al. Multiple HA substitutions in highly pathogenic avian influenza H5Nx viruses contributed to the change in the NA subtype preference. Virulence. 2022;13(1):990–1004. doi:10.1080/21505594.2022.2082672

[38] Patil A, Anhlan D, Ferrando V, et al. Phosphorylation of influenza A virus NS1 at Serine 205 Mediates Its Viral Polymerase-Enhancing Function. J Virol. 2021;95(6):10–128. doi:10.1128/JVI.02369-20

[39] Zhang Y, Sun Y, Sun H, et al. A single amino acid at the hemagglutinin cleavage site contributes to the pathogenicity and neurovirulence of H5N1 influenza virus in mice. J Virol. 2012;86(12):6924–6931. doi:10.1128/JVI.07142-11

[40] Luczo JM, Stambas J, Durr PA, et al. Molecular pathogenesis of H5 highly pathogenic avian influenza: the role of the haemagglutinin cleavage site motif. Rev Med Virol. 2015;25(6):406–430. doi:10.1002/rmv.1846

[41] Matsuoka Y, Swayne DE, Thomas C, et al. Neuraminidase stalk length and additional glycosylation of the hemagglutinin influence the virulence of influenza H5N1 viruses for mice. J Virol. 2009;83(9):4704–4708. doi:10.1128/JVI.01987-08

[42] Nataraj R, Chandra A, Kesavardhana S. Avian influenza virus neuraminidase stalk length and haemagglutinin glycosylation patterns reveal molecularly directed reassortment promoting the emergence of highly pathogenic clade 2.3.4.4b A (H5N1) viruses. bioRxiv. 2024:2024.05.22.595329.

[43] Chen S, Miao X, Huangfu D, et al. H5N1 avian influenza virus without 80–84 amino acid deletion at the NS1 protein hijacks the innate immune system of dendritic cells for an enhanced mammalian pathogenicity. Transbound Emerg Dis. 2021;68(4):2401–2413. doi:10.1111/tbed.13904

[44] Yamayoshi S, Kiso M, Yasuhara A, et al. Enhanced replication of highly pathogenic influenza A(H7N9) virus in humans. Emerg Infect Dis. 2018;24(4):746–750. doi:10.3201/eid2404.171509

[45] Zhang X, Xu G, Wang C, et al. Enhanced pathogenicity and neurotropism of mouse-adapted H10N7 influenza virus are mediated by novel PB2 and NA mutations. J Gen Virol. 2017;98(6):1185–1195. doi:10.1099/jgv.0.000770

[46] Good MR, Fernández-Quintero JW, L M, et al. A single mutation in dairy cow-associated H5N1 viruses increases receptor binding breadth. bioRxiv. 2024:2024.06.22.600211.

[47] Kristensen C, Jensen HE, Trebbien R, et al. The avian and human influenza A virus receptors sialic acid (SA)-α2,3 and SA-α2,6 are widely expressed in the bovine mammary gland. bioRxiv. 2024:2024.05.03.592326.

[48] Ríos Carrasco M, Gröne A, van den Brand JMA, et al. The mammary glands of cows abundantly display

receptors for circulating avian H5 viruses. bioRxiv. 2024:2024.05.24.595667.

[49] Jang H, Boltz D, Sturm-Ramirez K, et al. Highly pathogenic H5N1 influenza virus can enter the central nervous system and induce neuroinflammation and neurodegeneration. Proc Natl Acad Sci U S A. 2009;106(33):14063–8. doi:10.1073/pnas.0900096106

[50] Jang H, Boltz D, McClaren J, et al. Inflammatory effects of highly pathogenic H5N1 influenza virus infection in the CNS of mice. J Neurosci. 2012;32 (5):1545–1559. doi:10.1523/JNEUROSCI.5123-11.2012

[51] Ji ZX, Wang XQ, Liu XF. NS1: a key protein in the "game" between influenza a virus and host in innate immunity. Front Cell Infect Microbiol. 2021;11:670177. doi:10.3389/fcimb.2021.670177

[52] Penn R, Tregoning JS, Flight KE, et al. Levels of influenza A virus defective viral genomes determine pathogenesis in the BALB/c mouse model. J Virol. 2022;96(21):e01178-22. doi:10.1128/jvi.01178-22

[53] Te Velthuis AJW, Long JC, Bauer DLV, et al. Mini viral RNAs act as innate immune agonists during influenza virus infection. Nat Microbiol. 2018;3 (11):1234–1242. doi:10.1038/s41564-018-0240-5

[54] Turner DL, Bickham KL, Farber DL, et al. Splenic priming of virus-specific CD8T cells following influenza virus infection. J Virol. 2013;87(8):4496–4506. doi:10.1128/JVI.03413-12

[55] Halwe NJ, Cool K, Breithaupt A, et al. H5N1 clade 2.3.4.4b dynamics in experimentally infected calves and cows. Nature. 2024;637(8047):903–912. doi:10.1038/s41586-024-08063-y

[56] Guan L, Eisfeld AJ, Pattinson D, et al. Cow's milk containing avian influenza A (H5N1) virus—heat inactivation and infectivity in mice. N Engl J Med. 2024;391(1):87–90. doi:10.1056/NEJMc2405495

[57] Ly H. Highly pathogenic avian influenza H5N1 virus infections of dairy cattle and livestock handlers in the United States of America. Virulence. 2024;15 (1):2343931. doi:10.1080/21505594.2024.2343931

[58] Evolution of H5N1 avian influenza viruses in Asia. Emerg Infect Dis. 2005;11(10):1515–1521. doi:10.3201/eid1110.050644